POLITEKNIK NEGERI BALI

Journal of Engineering Design and Technology

logic

Vol. 24 No. 3 November 2024

LOGIC

Jurnal Rancang Bangun dan Teknologi

p-ISSN. 1412-114X

e-ISSN. 2580-5649

LOGIC

Jurnal Rancang Bangun dan Teknologi

Journal of Engineering Design and Technology

Gedung P3M, lt.1 Politeknik Negeri Bali, Bukit Jimbaran
PO BOX 1064 Kuta Selatan, Badung, Bali - Indonesia
Telp. (+62)361 701981 Fax. (+62)361 701128
Email: logic@pnb.ac.id

LOGIC JOURNAL TEAM

PREFACE

Logic: Jurnal Rancang Bangun dan Teknologi (Journal of Engineering Design and Technology) is a peer-reviewed research journal aiming at promoting and publishing original high quality research in all disciplines of engineering and applied technology. All research articles submitted to Logic should be original in nature, never previously published in any journal or presented in a conference or undergoing such process across the world. All the submissions will be peer-reviewed by the panel of experts associated with particular field. Submitted papers should meet the internationally accepted criteria and manuscripts should follow the style of the journal for the purpose of both reviewing and editing.

Logic is a journal covering articles in the field of civil and mechanical engineering, design, and technology published 3 times a year in March, July, and November. Language used in this journal is English.

LOGIC. P-ISSN 1412-114X
LOGIC. E-ISSN 2580-5649
Indexing : GOOGLE SCHOLAR, DOAJ, EBSCO OPEN SCIENCE DIRECTORY, SINTA, GARUDA

Best Regard,

LOGIC Editorial Team

TABLE OF CONTENTS

LOGIC
Journal of Engineering Design and Technology
Vol. 24 No.3 month November 2004 ; p. 101-109

p-ISSN : 1412-114X
e-ISSN : 2580-5649
http://ojs2.pnb.ac.id/index.php/LOGIC

TORQUE (PERFORMANCE) ANALYSIS, EXHAUST GAS EMISSIONS, AND EXHAUST FLOW MODELING VARIATION OF CATALYTIC CONVERTER FILTER NUMBER

Hajar Isworo[1], Kurnia Dwi Artika[1], Muhammad Khalil[1], Imron Mustofa[1]

1) Automotive Technology Department. Politeknik Negeri Tanah Laut, Kec. Pelaihari, Kabupaten Tanah laut, Kalimantan Selatan

Abstract. In a combustion engine, to generate torque, a combustion and compression process is required. Apart from obtaining mechanical energy, the combustion results also produce exhaust emissions, which can result in a polluted environment. This research aims to determine the influence of torque and exhaust gas emission modeling by using variations in the number of filters using simulation software. This research is descriptive and quantitative research with an experimental method. This research uses a Dyno test tool and a Gas Analyzer from this research to find out data from the exhaust that has been varied. The addition of a filter reduces the torque value by 1.7%. The presence of a filter on the catalytic converter has been proven to reduce levels of exhaust emissions that are harmful to the environment (CO, HC). Of the variations in the number of catalytic converters, filter number 2 is the best, producing 9.71 hp with CO emission levels of 1.7% and HC 553 PPM.

Keywords : catalytic converter, emission, torque, filters

1. INTRODUCTION

Most of the pollution and air pollution is caused by exhaust gases from vehicles which are currently expanding at an alarming rate. From the activities of motorized vehicles using petroleum fuel, CO, HC, and NOx exhaust gases are produced. Exhaust gas from combustion can produce air pollution. This study has been devoted to the investigation of the use of an exhaust gas energy recovery system in a test bench of a single-cylinder diesel engine in four different modes of operation, in search of the potential for recovery energy in these classes of devices, the influence of fuel on their efficiency and the influence of the device in the reduction of polluting emissions. For this reason, a thermoelectric generator is constructed, which is mainly made up of an internal rectangular duct-type heat exchanger and twenty thermoelectric modules installed on the upper and the lower side of the heat exchanger in a 5×2 arrangement. A data acquisition system is connected to the thermoelectric generator and it allows monitoring of the electrical power generated by the thermoelectric modules, the temperatures of the exhaust gases at the inlet and outlet of the heat exchanger, and the polluting emissions. The maximum net electrical power recovered was 65.28 W and 57.8 W for the B5 and the B10, respectively. The maximum value of energy recovery obtained leads to a decrease in fuel and a reduction in CO2, CO, HC, NOx, and NO emissions of 2.43% and 2.65% for B10 and B5. [1]

This investigation experimentally examines the influence of hydroxy gas fumigation in a diesel engine fueled with a biodiesel blend derived from waste palm cooking oil (B10). For the experimental tests, a fixed rotation speed of 2000 rpm and a load condition of 50%, 75%, and 100% have been established. Hydroxy gas (HHO) has been added through the engine's air intake system at a flow of 0.5 lpm, 0.75 lpm, and 1 lpm. Results have demonstrated the positive effect of HHO fumigation on the combustion performance of the B10 blend. Moreover, a reduction of 4.3% in the BSFC and a 2.64% increase in peak pressure in B10 due to the presence of HHO have been observed. On the other hand, a decrease of 8.7%, 9.9%, and 22.8% in CO2, HC, and smoke opacity emissions has been evidenced with the addition of HHO in B10. B10 implementation has promoted NOx emission escalation. However, this increase has been only 1.23% compared to pure diesel. In conclusion, HHO

enrichment favors combustion performance and emissions minimization, which represents a significant opportunity to mitigate the negative effect of the lower calorific power of these types of fuels. [2]

This study investigates the influence of biodiesel blends produced from agro-industrial residues of palm oil (Elaeis guineensis), on the performance and emission characteristics of a small-diameter single-cylinder diesel engine. The engine tests have been performed at three different loads with a constant speed of 3600 rpm. Experimental results have shown that the blends of biodiesel PB5 and PB10 cause a consumption of 1.12% and 2.45% higher than diesel. The addition of biodiesel from palm oil residues has allowed the reduction of CO, CO2, and HC emissions by 28.6%;12.6%, and 14.3%. However, biodiesel has caused an increase in Nox emissions and smoke density. The evaluation of the thermal efficiency of the brake has shown a difference of 2.4% and 3.7% for PB5 and PB10 compared to conventional diesel. Similar efficiency compared to diesel and significant reductions in CO, CO2, and HC emissions, show that biodiesel blends produced from palm oil agro-industrial wastes have the potential to partially replace the diesel content in the fuel, thus contributing to the reduction of engine emissions and reduce the environmental pollution caused by this type of waste. [3]

The high cost of extending national grid to the highly dispersed Fiji Islands has made many locations to be without electricity. Therefore, a techno-economic assessment of standalone (solar PV, diesel generator) and hybrid solar PV-diesel generator systems in four different regions of Fiji Islands has been carried out. The potential reduction in greenhouse emissions of a standalone diesel generator has been estimated and compared with that of the hybrid system. Solar radiation data for the four selected locations (Ba, Suva, Labasa, and Rakiraki) have been fed into the Homer software for analysis. This study is a comparative study of the four selected locations. Only the current price of diesel of $0.8 and the mean radiation of 5.64; 5.13; 4.79 and 5.22 kWh/m^2-day for the four selected locations, respectively, have been used thus there has been no variation in the value of these factors. It has been shown that Ba is the best location with the least levelized cost of energy of $0.4976/kW, while the highest levelized cost of energy of $0.5734/kW has been obtained for Rakiraki for a standalone PV solar energy system. The obtained findings can be a useful guide to stakeholders in Fiji and the world at large for effective energy planning. [4] Many developing countries are opting to rely on coal-fired power mainly due to the abundance of the resource and its economic viability since the capital needed to build a new coal-fired power plant is not as large as a nuclear power plant. Compared to nuclear power, coal-fired power does not bear the risk of major catastrophe and therefore it will be relevant in the power industry for many years to come. However, the major drawback of coal-fired power plants is the fact that it is not a clean energy prospect and it is considered one of the main contributors to the world's greenhouse gases. Coal combustion is usually associated with the emission of greenhouse gases such as CO, CO2, NOx, and SO2. One of the main objectives of coal combustion research is to develop techniques that will help power plant operators to utilize coal cleanly and efficiently by adopting coal blending practices. Currently, emission mitigation and boiler cleanliness issues through the coal blending process are focusing more on laboratory scale tests and not utilizing actual plant data and behavior. This study evaluates the effectiveness of the implementation of the Coal Combustion Prediction Analysis Tool (CPAT) as a tool to facilitate power plant operators in predicting the impact of individual or blended coal quality. It will provide early predictions on boiler combustion performance related to the coal quality and it will assist the power plant operators preparing for boiler process control optimization. This study will also discuss slagging and fouling factors of different coal type, which are used in one coal-fired power plant in Southeast Asia. [5]

Fuel quality is an important indicator for the efficient operation of SI engine. Gasoline fuel is produced in many countries under specifications that did not meet the standard specifications that negatively affect engine operation efficiency. Hence, in this study, the impact of Methyl tertiary butyl ether addition to local low octane gasoline on the performance of spark ignition engines and exhaust emission characteristics has been investigated. The fuel samples prepared with additive ratio selected by 5%, 10% and 15% in addition to local gasoline as a comparison threshold. Engine test has been performed and the resulted data collected at constant engine load and increasing speed. Study results reveal noticeable improvement in engine brake power and BSFC at medium and high engine speed with MTBE additive and the maximum improvement obtained with the addition of 10% MTBE to local gasoline at 3000 rpm engine speed. Increasing MTBE additive with local gasoline results in reducing HC and CO emission for all ratios and the minimum value of these emissions obtained with 15% MTBE over the whole engine speed with an increase in CO2 emission. Based on the obtained results, introducing MTBE at 10% additive ratio is suitable to improve the engine performance and mitigate the engine emissions compared to local low octane gasoline. 6]. The addition of a catalytic converter in motor vehicles has been proven to reduce exhaust emissions. The addition of a catalytic converter in motor vehicles has been proven to reduce exhaust emissions. However, the addition of filters to the catalytic converter that is excessive can reduce engine performance[7][8][9][10].

Research on catalytic converters using experimental tests can determine the content of CO2, CO, HC, and O2, as well as determine engine performance. Visual modeling using engineering software can explain the phenomenon of exhaust gas flow in the catalytic converter [11] [12]. Catalytic converters on standard motorbikes do not use plate filters, plate filters that use metal can attract CO and HC emissions. From here the researchers raised the issue of how much influence the number of plate filters has on exhaust gas emission levels and their

performance values [13].

This study discusses the effect of the number of catalytic converter filters on a 150cc motorcycle on torque values and modeling exhaust gas analyzers using Ansys software. For further research, it is possible to develop catalytic analysis on automobiles and heavy equipment, and variables will also be added that affect exhaust quality and improve performance, of course with the addition of data and variables a statistical analysis is needed to get the best composition [12][11][14][15]. The purpose of this research is to obtain minimum exhaust emissions and maximum engine performance.

2. METHODS

2.1 Tools & Materials

A. Tools

- dyno test

Figure 2 Diyno test for performance tester

Tool specifications:
Maximum power 200 HP
Drum Diameter 305 mm
Total weight 350 kg
Year of use 2020

Dyno test is a test that is used to determine the performance of a vehicle's motor.

- Motorcycle 150 cc

Figure 3 motor cycle 150 cc

-Gas Analyzer

Figure 4 gas emissinon Analyzer

Gas analyzer is an instrument or device used to measure the proportion and composition of combined gases. The function of the gas analyzer is to monitor exhaust emissions of CO, CO2, HC, and O2 by continuously measuring emissions.

-Catalytic converter

Figure 5 catalytic converter

2.2 Dimension catalytic converter

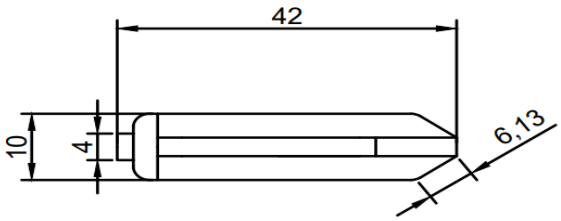

Figure 6 catatalic converter using one filter

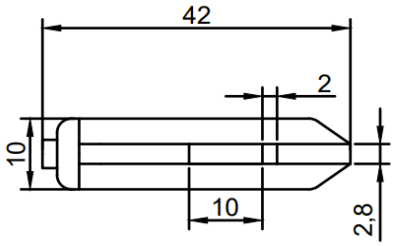

Figure 7 catalytic converter using two filters

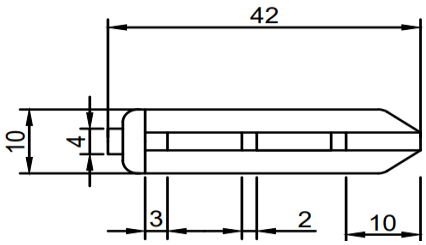

Figure 8 Catalytic converter using three filters

Units: millimeter

2.3 Boundary Condition

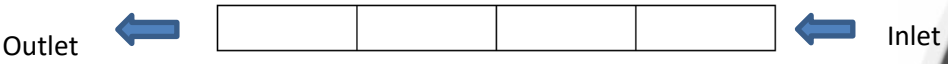

Figure 9 Boundary Condition Catalytic converter

2.4 Research Diagram

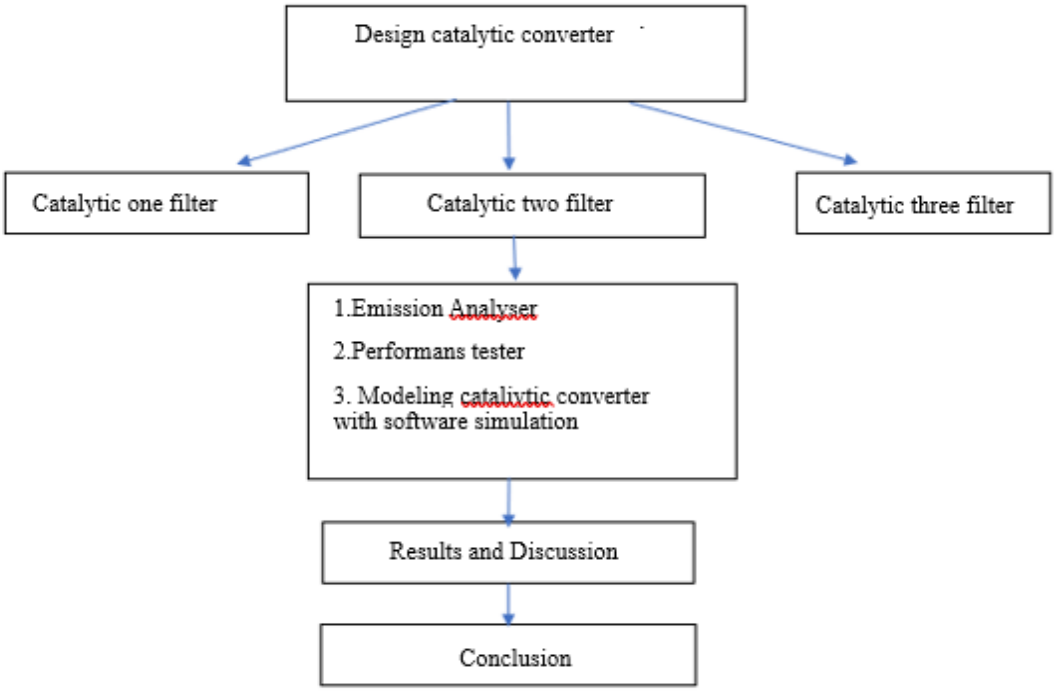

Figure 10 Research Diagram

3. RESULTS AND DISCUSSION

3.1 Performance Data Result

In the torque experiment, it was obtained using data obtained from the dynotest test.

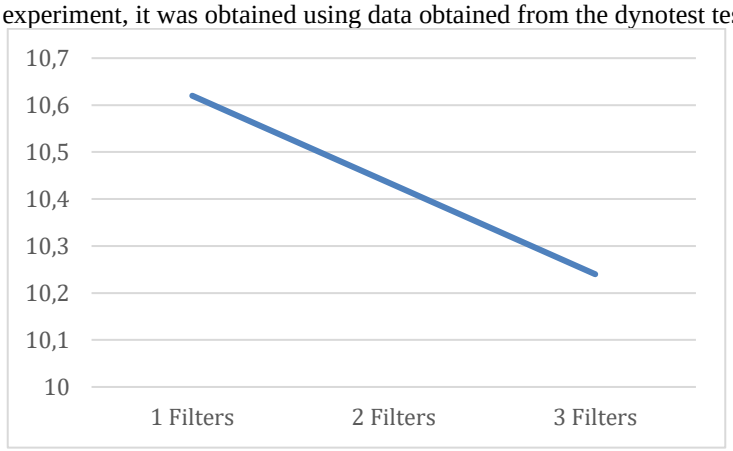

Figure 11 Number of filters vs Torque Value

The data above is, the results of taking the Dyno test where the data shows that for the results of the catalytic converter using 1 filter, the torque value was 10.30 N.m, and the catalytic converter using 2 filters obtained a torque value of 9.60 N.m. Meanwhile for 3 filters obtained a torque of 9.37 N.m. For 3 filters, the minimum torque produced is due to the large number of filters installed. The air coming out of the engine is not free to come out, so the resulting torque value is small.

Figure 12 the Relationship between Number of Filters-Engine Revolutions

The data above is, the results of taking the Dyno test where the data shows that for the results of the catalytic converter using 1 filter, the rotation value was 6.84 rpm. The catalytic converter using 2 filters obtained a rotation value of 6.13 rpm. Meanwhile, the 3 filters obtained a rotation of 5.94 rpm. For 3 filters, the minimum torque produced is due to the large number of filters installed. The air coming out of the engine is not free to come out, so the resulting rotation value is small.

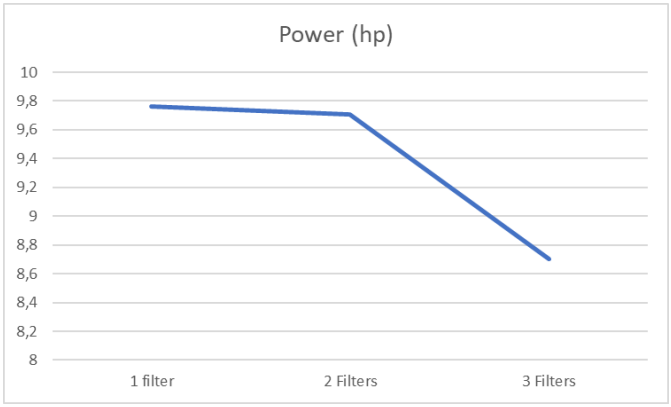

Figure 13 of the relationship between the number of filters and machine power

The following is a graph from the Dyno test where the data shows the highest results, namely 1 filter where the data produced power was 9.76 hp and filter 2 was 9.71 hp, for the lowest data, namely on 3 filters which only produced 8, 7 hp.

3.2 Emission Test Data Results

In the process of taking Emission Data obtained from the Analyzer.

Content of CO exhaust emissions

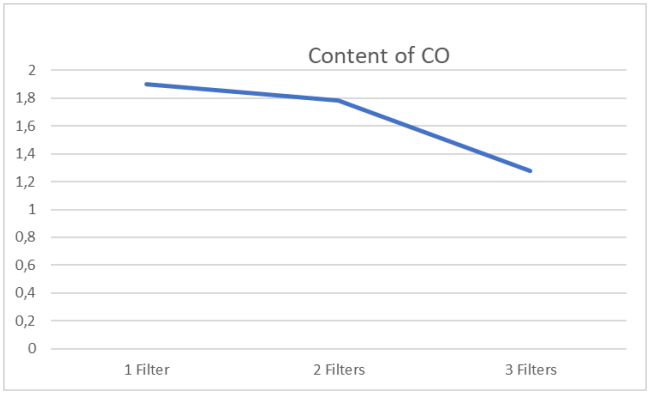

Figure 14 Number of filters-Content of CO (%)

From the graph above, it shows that the highest CO exhaust gas emission content was obtained in 1 filter, with a content of 1.9% and for 2 filters the data produced was 1.78% and for the lowest CO content, namely in 3 filters, it was 1.28%. The greater the number of filters, the lower the CO levels produced, meaning that the increase in the

number of filters has an effect on the CO2 levels.

Content of CO2 exhaust emissions

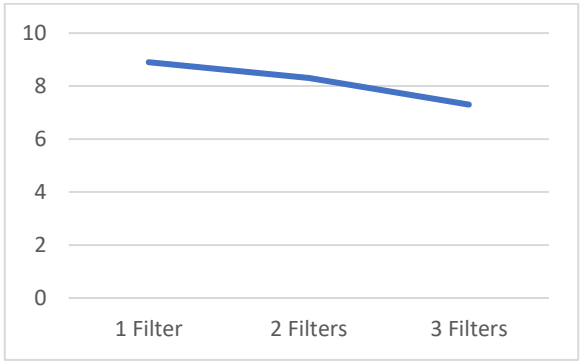

Figure 15 Number of filters-Content of CO_2 (%)

This graph shows that the CO2 content from exhaust gas emissions has the highest content in 3 filters at 8.90%, while for 2 filters it is 8.30% and the lowest content is in 1 filter at 7.30%. This graph shows that the best data is for 3 filter because CO2 can be filtered perfectly.

Content of HC exhaust emissions

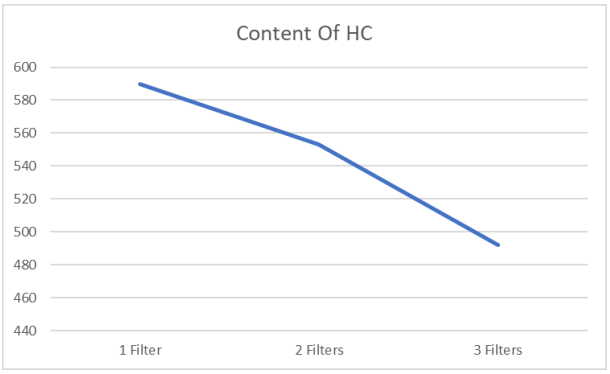

Figure 16 Number of filters-Content of HC (ppm)

Graph 4 shows the highest data obtained on 1 filter of 590 ppm, on 2 filters of 553 ppm, and on 3 filters of 492 ppm. Increasing the number of filters can reduce HC levels.

Content of O_2 exhaust emissions

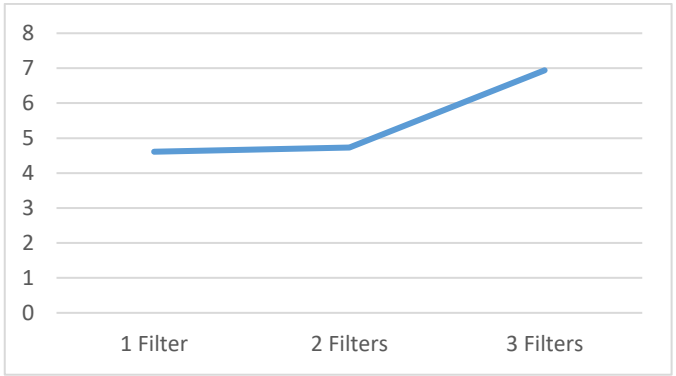

Figure 17 Number of filters-Content of O_2 (%)

Graph 17 shows that 1 filter is 4.61% and 2 filters is 4.73% and 3 filters is 6.94%. Increasing the number of filters can increase O2 levels.

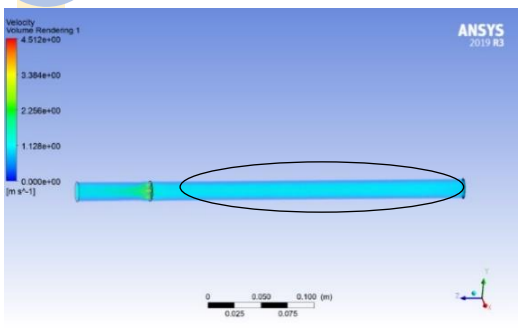

(a) Velocity 1 filter

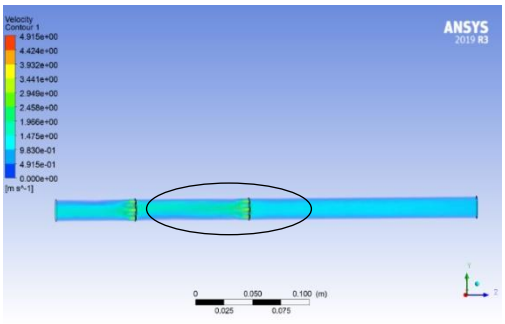

(b) Velocity 2 filters

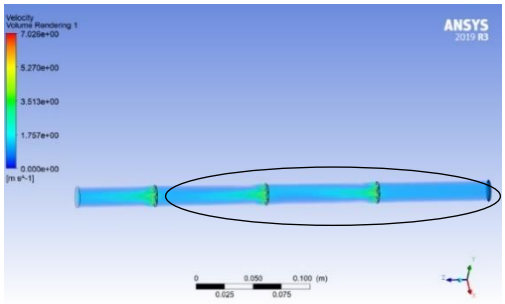

(c) Velocity 3 filters

Figure 18 Simulation results Velocity 1Filter, 2 Filters and 3 filters

Simulation analysis of exhaust gas velocity for filter 1, filter 2, and filter 3. As seen in Figure 18 (a) the speed of the inlet side is 3.384 m/s, then in Figure 18 (b) the speed of the inlet side is 1.966 m/s, and in Figure 18 (c) the speed of the inlet side is 1.757 m/s. From the inlet speed data, it can be concluded that the more the number of filters, the lower the catalytic converter inlet speed.

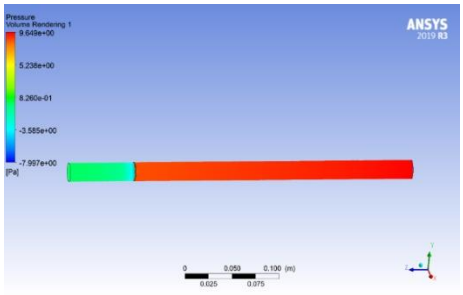

a) 1 Filter

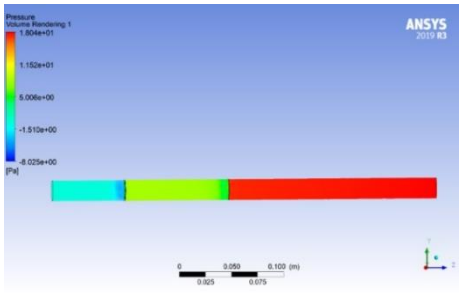

b) 2 Filters

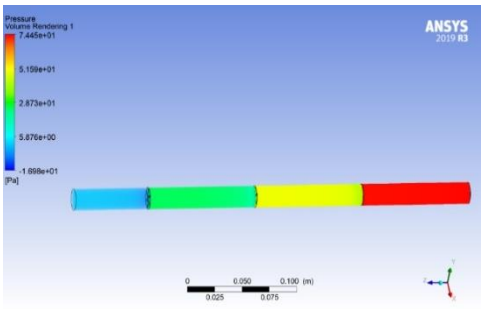

c) 3 Filters

Figure 19 Simulation results Pressure 1Filter, 2 Filters and 3 filters

You can see in picture (a) the pressure on the inlet side is 9.64 Pascal and on the outlet side the value is -7.997 Pascal, then Figure 19 (b) the pressure on the inlet side is 18.04 and the pressure on the outlet side is -8.025 and

in Figure 19 (c) the pressure on the inlet side is 7.445 and on the outlet side it is -16.98 Pascal. The use of filter number 3 is not recommended because on the outlet side, there is excessive back pressure, the value increases by 112.3% of the pressure of filter number 1. Excessive back pressure can reduce engine performance (see performance test results in Table 3).

Tabel 3 Velocity-Pressure

Catalytic	Velocity (m/s)	Pressure (Pascal)
1 Filter	4.51	9.65
2 Filters	4.91	18.04
3 Filters	7.02	74.45

4. CONCLUSION

a) The more filters there are in the exhaust, the lower the power produced
b) The presence of a filter on the catalytic converter has been proven to reduce levels of exhaust emissions that are harmful to the environment (CO, HC).
(c) Of the variations in the number of catalytic converters, filter number 2 is the best, the power produced is 9.71 hp with a CO emission level of 1.7% and HC 553 PPM

Based on the results of the Acceleration and Emission tests that have been carried out, the authors suggest several things, including;

a) Before performance testing, make sure the vehicle to be used is in good condition
b) When testing, don't forget to calibrate the tool before use.

5. REFERENCE

[1] W. Orozco, N. Acuña, and J. D. Forero, “Characterization of Emissions in Low Displacement Diesel Engines Using Biodiesel and Energy Recovery System,” no. 1, p. 2019.
[2] C. Pardo, J. A. Pabon, and M. Fonseca, “Performance , Emission , and Economic Perspectives of a Diesel Engine Fueled with a Mixture of Hydroxy Gas and Biodiesel from Waste Palm Cooking Oil,” no. 2, p. 2021.
[3] G. Prada, G. Valencia, and J. D. Forero, “Characterization of Emissions in a Diesel Engine Using Biodiesel Blends Produced from Agro-Industrial Residues of Elaeis Guineensis,” no. 1, p. 2020.
[4] O. M. Oyewola, O. S. Ismail, and M. O. Olasinde, “Techno-Economic Assessment and Potential Greenhouse Gas Emission Reduction of Standalone Solar PV and Hybrid Solar PV-Diesel Generator Systems in Fiji Islands,” no. 2, p. 2022.
[5] M. M. Mohammad Zahari Sukimi Mat Zaid(1*), Mazlan A. Wahid(2), “Coal Combustion Prediction Analysis Tool for Ultra Supercritical Thermal,” no. 2, p. 2020.
[6] J. I. Musa, O. M. Ali, and A. A. Hussein, “Analysis of SI Engine Operation and Emission Characteristics with Low Octane Gasoline and Ether Additive,” no. 1, p. 2022.
[7] T. Bajgude and A. Patel, “Design and Analysis of Catalytic Converter of Automobile,” p. 5.
[8] L. K. S.Ramasubramanian, M.Ganesh, “Design And Analysis Of Cataly c Converter Model With Shape Change For Overall Improvement In Fluid Flow,” vol. 8, no. 11, p. 8616.
[9] A. Ghofur *et al.*, “Modelling study of flue gas flow pattern with pressure, amount and shape variation catalytic converter,” *Arch. Mater. Sci. Eng.*, vol. 103, no. 1, pp. 5–17, 2020, doi: 10.5604/01.3001.0014.1769.
[10] Ghofur Abdul, Subagyo Rachmat, Isworo Hajar, “A study of modeling of flue gas patterns with number and shape variations of the catalytic converter filter,” *Energies*, vol. 6, no. 1, pp. 1–8, 2018, [Online]. Available: http://journals.sagepub.com/doi/10.1177/1120700020921110%0Ahttps://doi.org/10.1016/j.reuma.2018.06.001%0Ahttps://doi.org/10.1016/j.arth.2018.03.044%0Ahttps://reader.elsevier.com/reader/sd/pii/S1063458420300078?token=C039B8B13922A2079230DC9AF11A333E295FCD8.
[11] R. Rajendran, U. Logesh, N. S. Praveen, G. Subbiah, and A. Information, “Optimum design of catalytic converter to reduce carbon monoxide emissions on diesel engine,” 2020.
[12] R. W. Sudirman Rizki Ariyanto, Suprayitno, “Design of Metallic Catalytic Converter using Pareto Optimization to Improve Engine Performance and Exhaust Emissions,” p. 86.
[13] F. P. D. Patel a, Dattatraya Subedar b, “Design and development of automotive catalytic converter using non-nobel catalyst for the reduction of exhaust emission : A review,” 2022.
[14] R. U. L. S. P. S. Rajendran;, “Optimum design of catalytic converter to reduce carbon monoxide emissions on diesel engine,” 2020.
[15] S. Ramasubramanian, M. Ganesh, and L. Karikalan, “Design And Analysis Of Cataly c Converter Model With Shape Change For Overall Improvement In Fluid Flow,” vol. 8, no. 11, p. 8616, 2019.

LOGIC
Journal of Engineering Design and Technology
Vol. 24 No.3 November 2024; p. 110 - 116

p-ISSN : 1412-114X
e-ISSN : 2580-5649
http://ojs2.pnb.ac.id/index.php/LOGIC

FATIGUE TEST OF PLASTICS AND MANUFACTURING COLLET NUT DRIVER FOR INTEGRATED ROTATING BENDING FATIGUE TEST MACHINE

Tri Setyo Aji Cahyono [1)], Syamsul Hadi [2)], Rico Wahyu Pratama [3)], Zakiyah Amalia [4)], Fica Aida Nadhifatul Aini [5)], Aini Zuhra Binti Abdul Kadir [6)]

[1,2,3,4,5)] Mechanical Engineering Department, State Polytechnic of Malang, Jl. Soekarno-Hatta 9, Malang, Indonesia
[6)] Advanced Manufacturing Research Group, Faculty of Mechanical Engineering, Universiti Teknologi Malaysia, Johor Bahru, 81310, Malaysia

Corresponding email [2)] :
syamsul.hadi@polinema.ac.id
syampol2003@yahoo.com

Abstract. The unknown fatigue life of injection molded plastic materials and the ineffectiveness of clamping both ends of the specimen in the collet of the Integrated Rotary Bending Fatigue Testing Machine with manual tightening and loosening are the obstacles faced. The purpose of testing and making a collet nut driver is to obtain a prediction of the fatigue life of injection molded plastic materials and to increase the effectiveness of clamping the end of the specimen with the help of a DC motor drive. The research method uses experiments which include injection molding of plastic materials of the type Polypropylene (PP) and Acrylonitrile Butadiene Styrene (ABS), checking the straightness and surface finishing of the specimen, fatigue testing at 1800, 2000, 2200 rpm, analysis of fatigue test results, and design-manufacturing collet nut drive with DC motor drive and transmission of a pair of spiral cone gears, manufacture of DC motor sliding movement mechanism along the reach of both ends of the specimen, installation of electric power circuits for direction and electric current switches for clockwise and counterclockwise rotation functions, and analysis of the results of the fatigue test and performance of the collet nut driver The results of fatigue testing at a bending stress (S) of 68 MPa for PP material show that at 1800 rpm, the fatigue life (N) was obtained at 2,014,605 cycles and at 2200 rpm, N was obtained at 1,506,486 cycles. Meanwhile, for ABS specimens, at 1800 rpm, N was obtained at 1,547,106 cycles and at 2200 rpm, N was obtained at 1,190,425 cycles, which means PP material has a longer fatigue life compared to ABS. The test results of the DC motor drive on the collet nut showed that the duration of tightening/loosening was 4.4 times faster than manually, which originally had a duration of 66 seconds, down to just 15 seconds for the DC motor drive.

Keywords: Acrylonitrile Butadiene Styrene (ABS), Collet Nut Driver, Fatigue Life, Injection Molding, Polypropylene (PP).

1. INTRODUCTION

The use of plastic in modern society has increased rapidly [1], because plastic has advantages such as being strong, flexible, light, cheap and stable [2][3]. Most of the plastics used in the industrial world include Polypropylene (PP) plastic including waste [4] and Acrylonitrile Butadiene Styrene (ABS). This plastic is most widely used in everyday life, because it has good mechanical properties with low density, heat resistance, moisture resistance, and good dimensional stability [5]. PP and ABS plastics, including those printed with 3D [6-7], are widely used in car spare parts and have been proven to be able to balance car functions such as reducing weight and maintaining passenger safety [8]. One of the uses of PP plastic is rear fender products, while plastic (ABS) is applied to the front crossbar of the car as a bumper [9].

One of the tests to determine the fatigue life of a material is testing using a rotary bending fatigue machine [10-11]. The test is expected to be able to estimate the fatigue life of a component, the rotary bending fatigue machine

plays a very important role in fatigue testing.

Rotary Bending Fatigue is a test tool to determine the fatigue limit that occurs in materials, where fatigue occurs due to cyclical loading [12]. Fracture occurs because when the material has experienced a stress cycle which produces permanent damage as a process of permanent structural change at one point, it becomes the initiation of a crack, the spread of the crack and finally fracture which is carried out by varying loading methods [13]. The efficiency and effectiveness of these plastics is always a consideration in selecting materials according to their use.

With the widespread use of Additive Manufacturing in production, components made using Additive Manufacturing techniques can be used as components made using traditional/injection technology [14-15]. The process of making specimens was carried out using Additive manufacturing techniques using PP and ABS plastic ore. The specimens used follow the standard specimens from R.R. Moore [16].

The fatigue test method uses a rotary rod fatigue testing machine, as the specimen is gripped at both ends with a collet chuck and then the specimen is rotated at a certain speed with a load under the specimen, so that the specimen appears to receive cyclical or repeated loads. The availability of standard rotating bar fatigue testing machines whose functionality and affordability can support the ease of obtaining information about predicting the fatigue life of materials [17].

The position of installation and removal is very important in this test method, installation and removal of a fatigue test specimen that has broken after being fatigue tested, requires the operator to come to the fatigue test machine, after finding out via SMS sent by the machine when the specimen breaks. Manual installation requires certain skills so that the fatigue test can be carried out properly and does not slip during the fatigue test. In the future, it would be better if the broken specimen was replaced with a new specimen if it could be carried out automatically, the initial stage of designing the collet release and tightening was to use an automatic method, if it could be equipped with a robotic hand, however, the complete specimen replacement could be carried out automatically. Replacing a broken specimen with a new specimen semi-automatically requires a special construction design for the two collets on the existing integrated rotary bending fatigue testing machine.

2. METHODS

The research is a type of experimental research to test plastic materials that are often used in people's lives, namely PP plastic and ABS plastic. The research aims to determine the fatigue life of each material with the flow diagram is shown in Figure 1.

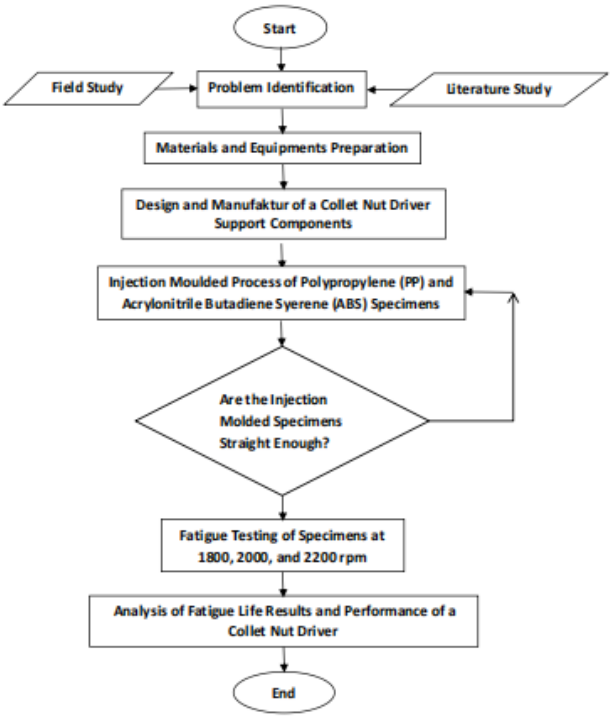

Figure 1. Research Flow Diagram

The research was carried out from March to July 2023 at the Materials Testing Laboratory on the 3rd Floor of the

Mechanical Engineering Building, Malang State Polytechnic, located at Jl. Soekarno-Hatta No. 9 Malang City, East Java. Integrated Rotary Bending Fatigue Testing Machine, FATEMACH is shown in Figure 2.

Figure 2. Fatigue Testing Machine, FATEMACH, Left Side View, Front View, and Right Side View

Fatigue life data in units of cycles obtained from testing for PP and ABS materials is directly recorded by the computer in the Integrated Rotary Bending Fatigue Testing Machine for the number of revolutions until the specimen breaks, while the load in units of kg given is recorded in the data entry to on the computer before the test includes the name of the material, the contact number of the operator who will send a short message (SMS) to the mobile phone, and the date. The bending stress is directly calculated by the computer and plotted directly in the form of an S-N curve. The shape of the collet nut and its installation on the spindle is shown in Figure 3.

Figure 3. The shape of the collet nut and its installation on the spindle

3. RESULTS AND DISCUSSION

In fatigue testing, installing specimens with manual collets requires skill and time in installing specimens using a 22 mm spanner and a 30 mm wrench with limited space, so it becomes less effective. By changing from a manual collet to a collet nut driver with the support of a DC motor and a pair of spiral cone gears, it can make it easier to install fatigue test specimens and save the time. The collet nut driver mounted on the integrated rotary bar fatigue testing machine table is shown in Figure 4.

Figure 4. Collet nut driver mounted on an integrated rotary bending fatigue testing machine table

The trial results of installing a specimen with 2 ends clamped manually using a 22 mm spanner and a 30 mm wrench took 66 seconds, while installing a specimen with 2 ends clamped with a collet nut driver assisted by a DC motor with a torque of 6 Nm requires a duration of only 15 seconds, which means its effectiveness is 4.4 times faster or only takes 22.7% of the time compared to manually installing specimens. The fatigue life of PP plastic is shown in Table 1 and Figure 5.

Table 1. Fatigue Life of PP Specimens

Specimen	Test Speed (rpm)	Load (kg)	S (MPa)	N (Cycles)	Duration (Minutes)
PP	1800	10	228	42327	21
		9	205	82255	45
		8	182	128739	73
		7	159	182553	104
		6	136	282164	160
		5	114	418613	239
		4	91	1305358	746
		3	68	2024567	1043
	2000	10	228	29439	15
		9	205	67482	34
		8	182	101469	62
		7	159	152547	90
		6	136	232912	148
		5	114	338455	221
		4	91	1233525	702
		3	68	1702591	1011
	2200	10	228	22371	10
		9	205	43034	30
		8	182	73784	56
		7	159	113045	85
		6	136	178515	136
		5	114	278258	180
		4	91	1056839	672
		3	68	1506486	936

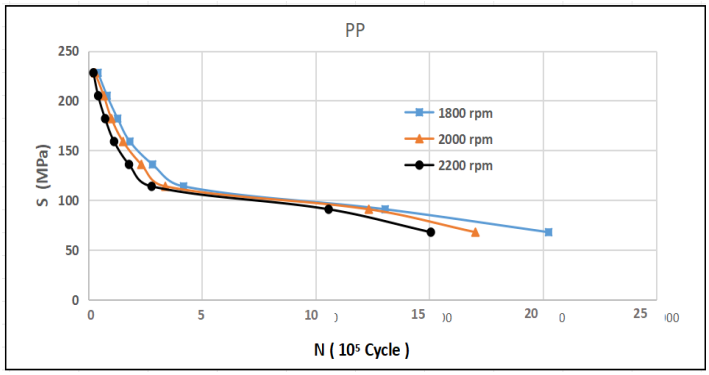

Figure 5. S-N Curve of PP

From fatigue testing on PP with test speeds of 1800 rpm, 2000 rpm, 2200 rpm, the data in Table 1 shows that PP material with a speed of 1800 with a load of 3 kg and a bending stress of 68 MPa has a longer fatigue life of 2014605 cycles with a duration of 1043 minutes, while for speeds of 2000 rpm and 2200 with a load of 3 kg with the same bending stress the fatigue life values are 1684536 cycles with a duration of 1011 and 1506486 cycles with a time of 936 minutes respectively. The fatigue life of PP plastic is shown in Table 2 and Figure 6.

Table 2. ABS Specimen Fatigue Life Table

Specimen	Test Speed (rpm)	Load (kg)	S (MPa)	N (Cycles)	Duration (Minutes)
ABS	1800	10	228	5459	4
		9	205	8336	6
		8	182	12562	9
		7	159	16324	12
		6	136	33840	16
		5	114	73258	37
		4	91	340979	205
		3	68	1547583	852
	2000	10	228	4868	3
		9	205	7456	4
		8	182	9651	6
		7	159	11751	9
		6	136	26676	13
		5	114	68558	44
		4	91	294643	178
		3	68	1317534	757
	2200	10	228	4037	2
		9	205	5905	2
		8	182	8384	4
		7	159	9991	5
		6	136	23851	12
		5	114	63880	51
		4	91	289660	185
		3	68	1190457	766

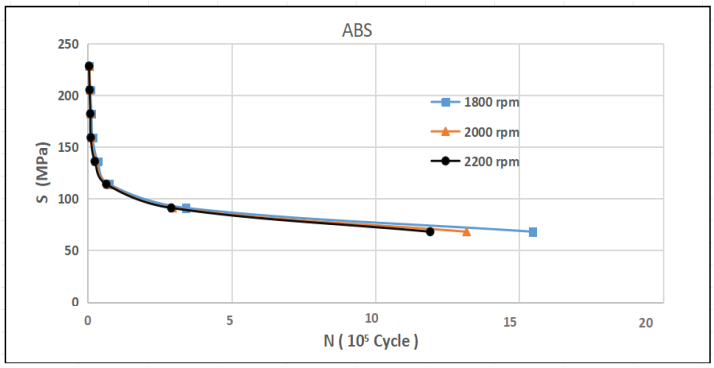

Figure 6. S-N Curve of ABS

From fatigue testing on ABS with test speeds of 1800 rpm, 2000 rpm, 2200 rpm, the data in Table 2 shows that ABS material with a test speed of 1800 rpm with a load of 3 kg and a bending stress of 68 MPa has a longer fatigue life of 1547106 cycles with duration of 852 minutes, while at speeds of 2000 rpm and 2200 with a load of 3 kg at the same bending stress the fatigue life values are 1317029 cycles with a time of 757 minutes and 1190452 cycles with a time of 766 minutes respectively.

4. CONCLUSION

Conclusions from the research results of fatigue tests on PP and ABS plastic materials as well as collet nut driver performance tests are:

1. The fatigue testing results at a bending stress (S) of 68 MPa for PP material indicate that at 1800 rpm, the fatigue life (N) was 2,014,605 cycles, while at 2200 rpm, N was 1,506,486 cycles.
2. The fatigue testing results at a bending stress (S) of 68 MPa for ABS material show that at 1800 rpm, the fatigue life (N) was 1,547,106 cycles, and at 2200 rpm, N was 1,190,425 cycles, demonstrating that PP material has a longer fatigue life (N) compared to ABS.
3. The performance test results of the collet nut driver with a DC motor drive show that the tightening/loosening duration is 4.4 times faster than manual operation, reducing the duration from 66 seconds to just 15 seconds when driven by a DC motor.

5. REFERENCES

[1] M. Azadi, A. Dadashi, S. Dezianian, M. Kianifar, S. Torkaman, and M. Chiyani, "High-cycle bending fatigue properties of additive-manufactured ABS and PLA polymers fabricated by fused deposition modeling 3D-printing," *Forces in Mechanics*, 3, pp.1-11, 2021. https://doi.org/10.1016/j.finmec.2021.100016

[2] A. J. Babafemi, B. Šavija, S. C. Paul, and V. Anggraini, "Engineering properties of concrete with waste recycled plastic: A review," *Sustainability*, MDPI, pp. 1-26, Oct. 2018. https://doi.org/10.3390/su10113875

[3] V. Saroha, B. S. Pabla, and S. S. Bhogal, "Characterization of ABS for enhancement of mechanical properties," *International Journal of Innovative Technology and Exploring Engineering*, vol. 8, no. 10, pp. 2164-2167, 2019. https://doi.org/10.35940/ijitee.J9379.0881019

[4] S. U. Handayani, M. Fahrudin, W. Mangestiyono, and A. H. M. Fadlu, "Mechanical properties of commercial recycled polypropylene from plastic waste," *Journal of Vocational Studies on Applied Research*, vol. 3, no. 1, pp. 1-4, 2021.

[5] R. Nazif, E. Wicaksana, and Halimatuddahliana, "Effect of Pyrolysis Temperature and Amount of Activated Carbon Catalyst on Yield and Quality of Liquid Fuel from PP Type Plastic Waste," *Journal of Chemical Engineering*, 5, pp. 49-55, 2016.

[6] M. M. Padzi, M. M. Bazin, and W. M. W. Muhamad, "Fatigue characteristics of 3D printed acrylonitrile butadiene styrene (ABS)," in: *4th AMMSE 2017 IOP Conf. Series: Materials Sci. and Engineering*, IOP Publishing, Tianjin, China, 269, p. 012060, 2017.

[7] Anonymuous, "Comprehensive Guide on Acrylonitrile Butadiene Styrene (ABS)," https://omnexus.specialchem.com/selection-guide/acrylonitrile-butadiene-styrene-abs-plastic last accessed on June 22, 2023.

[8] M. Sulaiman, U. Islam, and R. Rahmat, "Study of the Potential for Development of Polymer Composite Materials," *Mechanical Engineering National Seminar*, 2018.

[9] J. J. Mervin, M. Mariyappan, B. Ramesh, and M. S. Kumar, "Design and impact analysis of a jeep bumper made of composite material," in *IOP Conference Series: Materials Science and Engineering*, IOP Publishing, vol. 923, 2020. https://doi.org/10.1088/1757-899X/923/1/012015

[10] P. Costa, R. Nwawe, H. Soares, L. Reis, M. Freitas, Y. Chen, and D. Montalvão, "Review of Multiaxial

Testing for Very High Cycle Fatigue: From Conventional to Ultrasonic Machines," *Machines*, MDPI, Jun. 2020. https://doi.org/10.3390/MACHINES8020025

[11] P. Shreyas, M. A. Trishul, R. C. Kumar, K. R. K. Babu, "Testing of Al 7075 Specimen Using Dual Specimen Rotating Bending Fatigue Testing Machine," *Int. Advanced Research J. in Sci., Eng. and Tech.*, vol. 2, no. 4, pp. 11-13, 2015.

[12] Muharnif, M., & Septiawan, R. Fatigue Test Analysis of 304 Stainless Steel Material Using a Rotary Bending Fatigue Machine, *Journal of Materials, Manufacturing and Energy Engineering*, 1(1), 64–73, 2018. https://doi.org/10.30596/rmme.v1i1.2437

[13] Maryadi, and D. R. L. Hakim, "Redesign of the Rotary Bending Type Fatigue Test Equipment," *F. SAINTEK*, Unira Malang, vol. 6, no. 1, pp.23-31, Apr. 2022.

[14] M. Frascio, A. Massimiliano, M. Margeritha, "Fatigue Strength of Plastics Components Made in Additive Manufacturing: first experimental results," *Procedia Structural Integrity*, vol.12, pp. 32-43, 2018.

[15] M. J. W. Kanters, L. F. A. Douven, P. Savoyat, "Fatigue life prediction of injection moulded short glass fiber reinforced plastics," *Procedia Structural Integrity*, 19, pp. 698-710, 2019.

[16] S. Hadi, A. Murdani, and F. Rokhman, "Design, Fabricated, and Trial on a Fatigue Test Machine," *XVI Annual National Seminar on Mechanical Engineering Proceeding*, Surabaya, Indonesia, pp. PMT-39, 201-207, Oct. 2017.

[17] S. Hadi, A. Murdani, and A. Wicaksono, "Design and Manufacture a Tool Post for Turning the Fatigue Test Standard Specimen Profile for Plastic Materials," *XVII Annual National Seminar on Mechanical Engineering Proceeding*, Kupang, NTT, Indonesia, pp. PMT-11, 65-72, Oct. 2018.

LOGIC
Journal of Engineering Design and Technology
Vol. 24 No.3 November 2024; p. 117 - 128

p-ISSN : 1412-114X
e-ISSN : 2580-5649
http://ojs2.pnb.ac.id/index.php/LOGIC

THE EFFECT OF CHILLER AND HOT RUNNER TEMPERATURE ON APPEARANCE OF 100 mL PET BOTTLE PRODUCTS THROUGH THE STRETCH BLOW MOLDING PROCESS

Moh. Hartono[1)], Prihadi Mulya Pradana[2)]

1,2) Mechanical Engineering Departement, State Polytechnic of Malang, Jl Soekarno-Hatta 9, Malang, Indonesia

Correponding email [1)] : moh.hartono@polinema.ac.id

Abstract. The using of plastic in human life is increasing over time. This increase occurs because plastic is not easily broken, flexible, practical, economical, and can replace the function of other items. One of the plastic molding processes is Injection Stretch Blow Molding, a plastic molding machine method that combines two processes, namely injection molding and stretch blow molding. The injection stretch blow molding process is a plastic molding machine that is melted and then injected into the mold to form a preform that is stretched and blown to form the product. This machine has a high level of precision so that the aspects of strength and appearance quality on the packaging bottle are the main assessment. The aim of this research is to determine the effect of temperature parameters on black spots, stripes and stripes on 100 mL PET bottle products. It is necessary to handle chiller temperature, hot runner temperature as independent variables in printing preforms. The control variables are material composition, cycle time, holding time, and component gap position. This type of research is experimental research and the processing method used in this research uses the design of experiments using statistical software. The level of variation in hot runner temperature parameter settings is 265°C, 270°C, and 275°C and chiller temperature is 17°C, 18°C, and 19°C. From the results of this research, it can be concluded that the significant parameters used for the chiller are 18°C, the appearance defect is 0.2% and for the hot runner it is 270°C, the appearance defect is 0.4%. This number is a significant parameter that produces fewer appearance defects for 100 mL PET bottle products in order to reduce the number of rejects.

Keywords :Injection Stretch Blow Molding, chiller, hot runner, preform, appearance.

1. INTRODUCTION

The use of plastics in human life is increasing from time to time. This increase occurs because plastic is lightweight, unbreakable, flexible, practical, economical which can replace the function of other goods. Currently, the production capacity of the national plastic products industry reaches 7.679 million tons, and the total consumption of plastic finished products reaches 8.227 million tons. Of the total consumption of plastic finished products, 7.12 million tons are met domestically. The large amount of imported products to meet the needs of plastic finished products and raw materials for the plastic industry shows that there is still a need to increase production capacity and new investment in this sector to replace imported products [1].

The plastic molding process has various types of processes in processing raw ore into the final product. The types of plastic molding processes are injection stretch blow molding, blow molding, extrusion molding, and vacuum

molding, rotation molding. All of these types of processes are applied according to the material used and the shape of the product volume produced. For cosmetic and food packaging products tend to use injection stretch blow molding machines, one of the products produced is 100 mL PET bottles, it is necessary to conduct research on the treatment of temperature parameter settings because it has an influence on product results, besides that the composition of material ore, type of mold material, and volume of product molds also have an influence on product results.

Injection stretch blow molding is machine that focuses on cosmetic packaging products. Unique and elegant shapes are often judged in the stretch blow molding process. The molding process has a high level of precision so that aspects of strength and quality of appearance on the packaging bottle become the main assessment. So as to get results close to perfect value according to the production standards set by the company's Quality Assurance. It is necessary to handle the chiller temperature, hot runner temperature in printing the preform until it becomes a product, as well as adjusting the cycle time, holding time, and the position of the component gap. The purpose of the handling carried out is to reduce defects in products such as stripes, black spots, hair on the bottom of packaging bottles, and uneven dimensions. These defects can be seen visually and sampling of each production for organoleptic testing by Quality Assurance in the laboratory.

Organoleptic or sensory assessment is the most primitive way of assessment. Sensory assessment became a field of science after the assessment procedure was standardized, rationalized, linked to objective assessment, data analysis became more systematic, as well as statistical methods used in analysis and decision making. Organoleptic assessment is widely used to assess quality in the food industry and other agricultural products industry. Sometimes this assessment can give very precise assessment results. In some cases the assessment with the senses even exceeds the accuracy of the most sensitive tools [2]. Plastic molding molding companies have targets according to the vision and mission. Experimental treatment in the production process will have an impact on the production target timeline and the impression of consumers who work with the company. Based on the description of all aspects of plastic molding. In line with the vision of the plastic molding industry that wants the production process to be a professional company that excels.

2. METHODS

2.1 Types of Research

The data collection method in this study uses quantitative experimental methods. Furthermore, data analysis processing was carried out to determine the effect of the independent variable on the dependent variable using statistical software and DOE factorial experimental design.

2.2 Time of Research

This research was conducted from February to April 2024

2.3 Research Tool and Material

The tools and material used in this research include

1. Injection Stretch Blow Molding Machine [3].

Spesification Machine

- Standard Screw Diameter (φ) : 54 mm
- Theoretical Injection Capacity : 366*[3] cm^3
- Injection Clamping Force : 687 kN
- Blow Clamping Force : 242 kN
- Driving Power (Rated) : 33 kW
- Heater Capacity (Rated) : 25.8*[4] kW
- Oil Reservoir Capacity : 600 L
- Machine Size (L×W×H) : 5,643 ×1,896 ×3,208 mm
- Machine Weight (Approx.) : 9.0 Ton
- Numbers of cavity : 6

2. Plastic Material

The material used in making polyethylene terephthalate [4] (PET) 100%.

Figure 1. Polyethylene Terephthalate

3. Camera

Macro photography is a technique that can capture small objects, looks more interesting because the resulting perspective observed can be experimental data as well as documentation to show reality during research.

2.4 Research Variables

In the research, there are variables that play an important role in taking data during research, as in Table 1. Next:

Table 1. Research variables.

Independent variable		
1	Temperatur chiller (°C)	: 17°C, 18°C, and 19°C
2.	Temperatur hot runner (°C)	: 265°C, 270°C, and 275°C
Dependent variables		
1.	Quality Appearance Product (%)	
Controlled Variables		
1	Materials	: PET (polyethylene terephthalate)
2	Composition material	: 100 % original
3	Cycle time (t)	: 1.48 s
4	Pressure Inject (bar)	: 4.48
5	Holding time (t)	: 1.31 s

2.5 Research Hypothesis

The hypothesis in this research are:

Hypothesis Zero (H_0) : There is no effect of chiller temperature and hot runner on the appearance quality of 100 mL PET bottle products in the stretch blow molding process.

Hypothesis Alternative (H_1): There is an effect of chiller temperature and hot runner on the appearance quality of 100 mL PET bottles in the stretch blow molding process.

3. RESULTS AND DISCUSSION

3.1 Result

10 replications were carried out, the results of product identification and attribute data from the data collection process were 90 pieces of 100 mL PET bottle products for the normal standard of defects in 100 mL PET bottle products as a benchmark is no. 2 with a chiller temperature of 18°C and a hot runner temperature of 270°C which produces minimal defects shown in Table 2:

Table 2. Research results and observations

No	Temperature *Chiller* (°C)	Temperature Hot Runner (°C)	Product Result Appearance										Chance of Failure
			1	2	3	4	5	6	7	8	9	10	
1	17	265	1	1	1	1	1	1	1	1	1	1	1
		270	1	1	1	1	1	1	1	1	1	0	0,9
		275	0	0	0	0	0	0	0	1	1	1	0,3
2	18	265	1	1	1	1	0	0	0	0	0	0	0,4
		270	0	0	0	0	0	0	0	0	0	0	0
		275	0	0	0	0	0	0	0	0	1	1	0,2
3	19	265	1	1	1	1	1	1	1	1	1	1	1
		270	1	1	1	0	0	0	0	0	0	0	0,3
		275	1	1	1	0	0	0	0	0	0	0	0,3

From the data collection of 90 products, the product documentation data value 1 indicates the defective effect while 0 indicates no defect. The following figure 2 is a normal sample of 100 mL PET bottle without defects:

Figure 2. Good product

Figure 2 above is an example of a good product without defects in a 100 mL PET bottle as a reference, with optimal temperature settings and no problems in the production process machine. Data colection that has been carried out, then the data processing is continued using statistical software. The following are the result of the analysis that has been carried out:

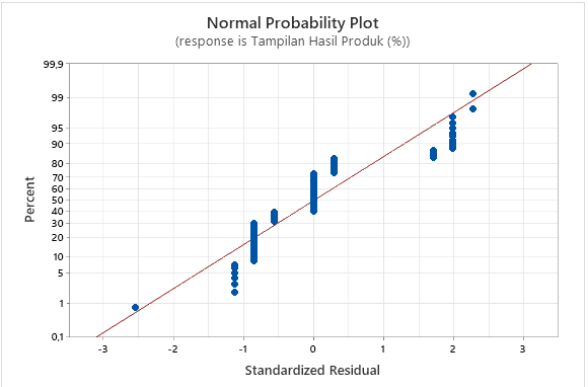

Figure 3. Grapich normal probability plot

The normal probability plot graph shows that the residual points formed are close to the red line. The significant value shown (P-Value> 0.05). If the significant value> 0.05 then the data is normally distributed. The results of the residual normality test can be said that the data follows a distribution that is close to normal. It is assumed that the regression model that has been made can be used.

Table 3. Analysis of variance

Source	DF	Adj SS	Adj MS	F-Value	P-Value
Model	8	11,289	1,4111	10,21	0,000
Linear	4	8,978	2,2444	16,23	0,000
Temperatur Chiller (°C)	2	4,356	2,1778	15,75	0,000
Temperatur Hot Runner (°C)	2	4,622	2,3111	16,71	0,000
2-Way Interactions	4	2,311	0,5778	4,18	0,004
Temperatur Chiller (°C)*Temperatur Hot Runner (°C)	4	2,311	0,5778	4,18	0,004
Error	81	11,200	0,1383		
Total	89	22,489			

The ANOVA table shows that the chiller temperature and hot runner temperature have an interaction value of P-value of 0.004 so that based on the hypothesis in this study the decision taken is to reject the initial hypothesis because the P-value is smaller than the alpha (α) tolerance level of 5% or 0.05 that has been set (p-value < alpha (α)). So that the null hypothesis (H0) is rejected and the alternative hypothesis (H1) is accepted, then the appearance defects on 100 mL PET bottles are also influenced by the hot runner temperature and chiller temperature significantly.

Table 4. Model summary

S	R-sq	R-sq(adj)	R-sq(pred)
0,371849	50,20%	45,28%	38,52%

The coefficient of determination (R-square) value aims to predict or see how much influence the independent variable contributes to the dependent variable. Based on the model summary above, it shows the coefficient of determination of 50.20%, the percentage value of the coefficient of determination is closer to 100%, it can be concluded that it has a significant influence. Approaching perfectly the total of the two independent variables used on the dependent variable, the R-sq number above means that the chiller temperature and hot runner temperature have an influence on appearance defects in 100 mL PET bottles of 50.20%, and the remaining half of 40.80% is caused by other variables not examined outside the regression. Then the variable that is not used in this study is known as error symbolized by (e).

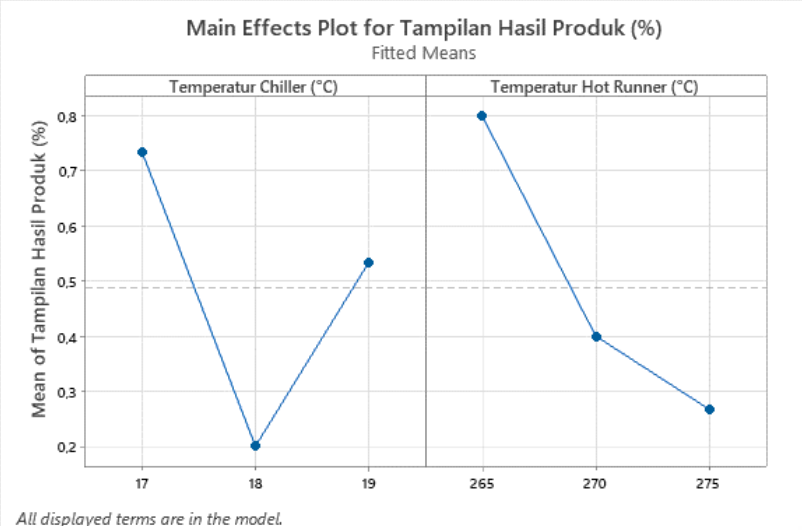

Figure 4. Main effect plot

Based on the results of this study, figure 4 factorial plot can be seen that the chiller temperature level of 17 °C has the most percentage defect opportunities with values between 0.7% to 0.8% the lower the chiller temperature level causes the product appearance defects to be large, at the chiller temperature there are striped defects, this is because at that temperature the preform has problems during the blow process, Likewise, the value of many defects is at a chiller temperature of 19 °C. The higher the chiller temperature level causes product appearance defects not to be safe because the character of each mold is not the same which can occur spotted and haired defects, while the

smallest chance of appearance defects worth 0.2% is in the temperature range between the two chiller temperatures, namely 18 °C.

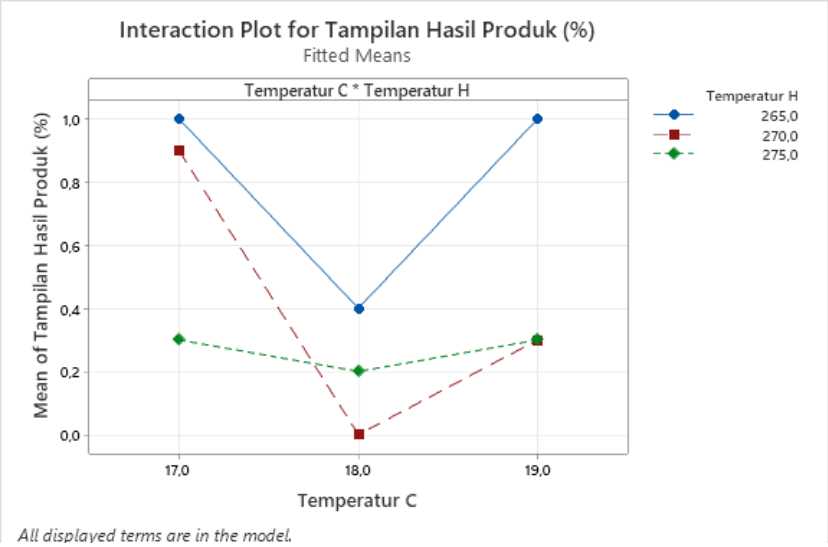

Figure 5. Graphic interaction plot

In figure 5 there are 3 kinds of colors and types of lines that indicate the hot runner temperature used. The first blue line is shaped like the letter V which indicates the level of use of the hot runner temperature of 265 °C, the second line is red dotted indicating the level of use of the hot runner temperature of 270 °C, then the last is a green short dotted line indicating the use of the hot runner temperature of 275 °C. Then the horizontal line across the graph shows the chiller temperature used with levels of 17 °C, 18 °C, and 19 °C. The vertical line shows the dependent variable that occurs or appearance defects in 100 mL PET products. Based on the figure 5 graph, it explains that the chances of defects in the appearance that occur are on the blue line, the lower the chiller temperature is set and the hot runner temperature of 265 °C the product will experience appearance defects, but if the chiller temperature is increased by 1 level to 18 °C, the defect decreases slightly to around 0.4%. However, when the chiller temperature is increased further, the defects increase significantly. The position of the right parameter setting is minimal or even 0 chance of defects shown on the dashed red line with a large value of 18 °C chiller temperature, but when the chiller temperature is lowered it experiences a steep graph approaching the blue line point defect of about 0.9%, the difference is that when the chiller temperature is increased to 19 °C the defect is not too high around 0.3% this figure is one point with a dashed red line. Then the short dotted green graph line shows a gentle slope, the low value of defective appearance on the product at 18 °C chiller temperature setting of 0.2%, when raised and lowered experiencing the same defect ratio. This means that of the three interactions of hot runner temperature levels, there is a low product display defect at the 18 °C chiller temperature level. Chiller temperatures at 17 °C and 19 °C show the same graph point results that occur on the blue line 1.0% and green 0.3%.

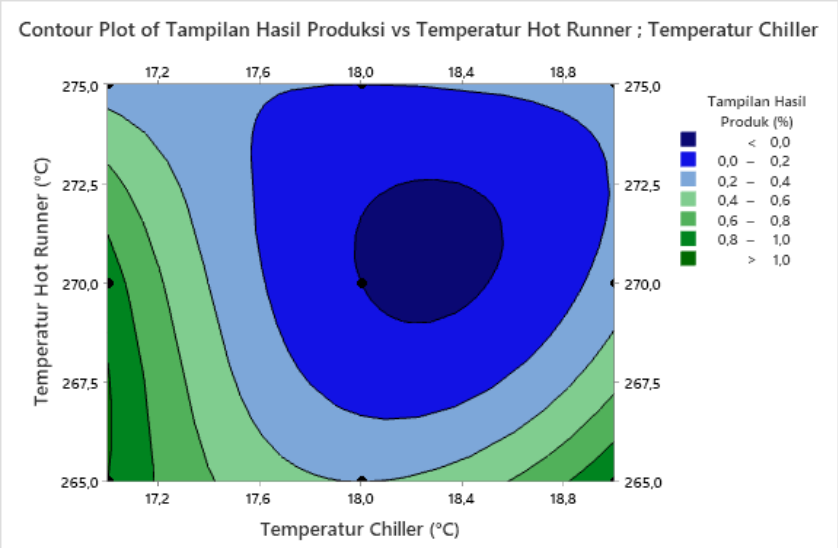

Figure 6. Graph contour plot

Based on figure 6, there are 7 different scale colors, but in the graph above that only 6 colors come out to find out the boundary area that occurs appearance defects in the product, there are 3 blue color degradation which indicates if the blue color is getting older then the chance of defects that occur will be even lower at 0 - 0.2%, it can also be seen with a black dot in the dark blue boundary line area showing minimal defective production, and there are also 3 green color degradation which states that the older the green color displays the starting level of appearance defects that occur will be higher. The contour plot graph above for the appearance defect of 100 mL PET bottle products is the lowest at 0 which is found in the darkest blue area, namely in the combination of chiller temperature of 18°C - 18.4°C and hot runner temperature of 269°C - 272.2°C. Meanwhile, the highest defect occurs in the area where the chiller temperature is 18 °C - 18.4 °C and the hot runner temperature is 269°C - 272.2°C. The highest defect occurs in the area where the chiller temperature is 18°C - 272.2°C. Meanwhile, the highest defect occurs in the darkest green area with a value of 1 which occurs in the combination of hot runner temperature of 265°C – 270°C and chiller temperature of 17°C - 17.2°C.

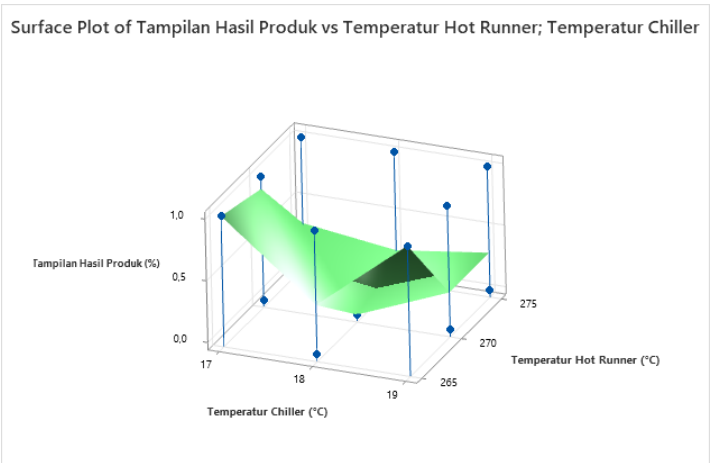

Figure 7. Graph surface plot

Figure 7 above displays a shape resembling a concave crater in the middle, meaning that at low chiller temperatures with low hot runner temperatures the chances of appearance defects in 100 mL PET bottles that occur will be higher located at temperatures of 19 °C and 265 °C depicted on a very high surface touching the number 1 on the chances of appearance defects results. Then the higher the temperature of the hot runner and chiller does not show a high steep surface like the effect at low temperatures, defects occur but are not too severe. Then the low concave shape in the middle of the graph that the stable level of temperature used between the two temperatures that can produce a minimum defect value scale even 0 product appearance on 100 mL PET bottles. so that the normal level of stable temperature temperature parameters has a significant sensitive interaction.

3.2 Discussion

Defects that Occur

Three types of appearance defects in accordance with the literature review which are influenced by the temperature of the hot runner and chiller are black spot, defect line, stripes. In this research, it is also in line with research conducted [5] entitled "Causes of Wavy Preforms and Their Effect on Bottle Products at PT Jayatama, Selaras, Bogor, West Java" the cause of wavy preforms, one of which can be influenced by machine factors, such as mold temperatures that are too high, chillers that are obstructed, and unstable heating systems. Various defects in products that occur in addition to the three types of appearance defects mentioned in the literature review in the form of black spots, hairly or defect lines, and stripes. There are also short shot, bubble or void, shrinkage, off center base, failed blowing, embossed bracelet, rough parting line.

1) Black spot

Black spots on the surface area of the bottle give rise to a dull, spotty appearance which is caused by one of the hot runner and barrel temperatures being too high, overheating, the material becomes burnt, and the material becomes contaminated with scale or small particles of dirt.

Figure 8. Black Spot Defect

2) Hairline defect

Hairline defect or defects on the bottom and neck of the bottle look like hair scratches, this is rare but occurs usually because the nozzle is dirty and the metal oring on the runner needs to be replaced combined with an incorrect cycle time.

Figure 9. Hairline defect.

3) Stripes

Stripes or opaque spots on the body of the bottle are cases that occur during production so that the color display is uneven, due to the interaction of temperature in the unstable material, making the color look uneven and streaky.

Figure 10. Stripes defect

4) Shrinkage

Shrinkage in thermoplastic undergoes a cooling process combined with changes in dimensions (shrinking) after the product is ejected out of the lip cavity in the injection stretch blow molding process. Shrinkage that occurs in thermoplastic materials is caused by compressibility and thermal expansion which usually occurs at the neck of the bottle, shrinkage defects also exist in the ISBM process but this rarely happens.

Figure 11. Shrinkage

5) Short shot

Short shot is a product defect caused by incomplete filling in the mold cavity. This is due to insufficient material being injected into the molding, insufficient injection pressure, lack of ventilation so that air is trapped in the cavity. This defect rarely occurs on ISBM machines because the preform used in the initial injection process does not immediately form a product on the machine.

Figure 12. Shrinkage

(Norman, 2021)[6]

6) Bubble

Bubbles are pockets of air bubbles that are trapped on the surface of the product. This defect occurs due to air humidity and the temperature of the material injected into the cavity mold when the clambing is being blown. Air does not have time to escape through the vents in the mold.

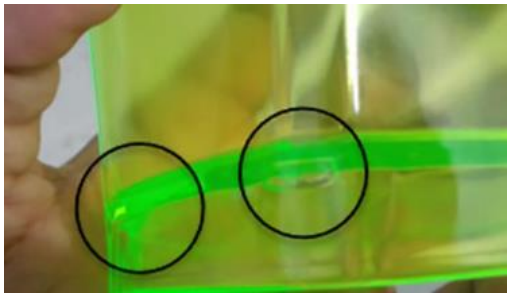

Figure 13. Bubble defect

(Diego, 2018)[7]

7) Bracelet defect

This defect in the bottle body ring on the inside occurs due to a lack of pressure from the air nozzle. There is a problem when the preform is blown into the mold cavity.

Figure 14. Bracelet defect

8) Slanted navel point (Off center base)

Slanted navel point (Off center base) This defect is because the initial shape is not yet standard. This occurs at an early stage during the stretching process of the preform before it is blown, causing the bottom of the bottle, the navel point or injection channel of the preform material to deviate from the middle. This defect also occurs because the wind pressure on the blow nozzle and the pen rod hits the bottom cavity. Meanwhile, the flexibility of the preform is not yet stable, so this defect is not caused by the influence of the temperature of the chiller, hot runner and preform heater.

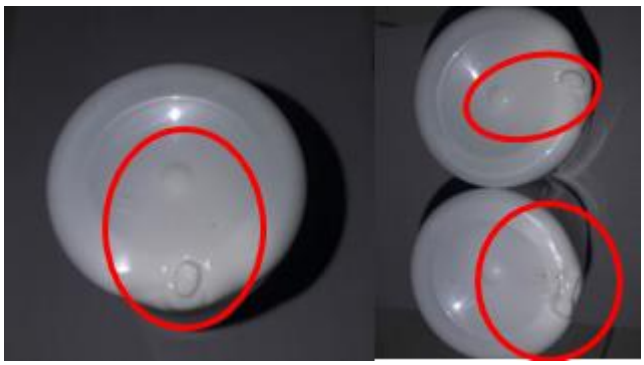

Figure 15. Slanted navel point (Off center base)

9) Failed blowing

Failure to blow is a defect because the initial shape cannot form a perfect bottle. This is influenced by the function of the preform pen rod whose position in the blowing cavity hits the preform until it penetrates [8], and the heating temperature or heating core does not reach the optimal temperature. These defects can be in the form of creased bottles, dents, stunted bottles, torn or leaking bottles.

Figure 16. Failure to blow

10) Rough joint line defect

Rough Parting Line is a defect that appears in the connecting line that occurs on the bottle body, this is because there is a problem with the cavity mold or the installation is not suitable. Dimensional defects are caused by component mechanisms and temperature parameter settings.

Figure 17. Rough joint line defect

The events in the research carried out produced an R-Squere figure of 50.20% and a p-value of 0.004. This figure shows that it is not synchronous, this is because the research data taken is attribute or defect data which in the data is in the form of visual defects. There is no measurement level for defects.

4. CONCLUSION

In researching the effect of chiller temperature and hot runner temperature in the plastic molding process on the appearance quality of 100 mL PET bottles, the conclusions obtained are:

1. The effect of the chiller temperature for the plastic molding process on the appearance quality is that the lower it is, the smaller it will cause defects in the form of lines or blurring due to poor preform formation making it difficult to blow. a chiller temperature of 17 °C produces a high level of product defects of 0.74%, and at a temperature of 19 °C product defects show a scale of 0.54%, this figure is in accordance with the mean factorial plot graph.
2. The effect of the hot runner temperature of the plastic molding process on the appearance quality is that the lower it is, the smaller it will cause defects in the form of black spots because the melted material is not stable evenly, and does not follow the heat from the screw barrel. The hot runner temperature at the level of 265 °C produces high product defects, namely 0.80 and the higher it will cause hairline defects on the bottle body because the material exceeds the melting limit in the 100 mL PET bottle preform. at 275 °C, product defects show a scale of 0.28%, this figure comes from the average factorial plot graph.
3. Research analysis of the interaction of the two independent variables, namely chiller temperature and hot runner temperature on the appearance quality of 100 mL PET bottles, shows that the actual optimal temperature rarely causes defects at the chiller setting of 18 °C and the hot runner setting of 270 °C in order to get the value results significant actual.

5. ACKNOWLEDGMENT

The author would like to thank Dr. Drs. Moh. Hartono, M.T. for the support and guidance that has been given. And thanks to all parties: parents, siblings and colleagues who have helped the author in completing this journal.

6. REFERENCES

[1] ASB, *One-Step Injection Stretch Blow Molding Machine ASB Series—ASB-70DPH ASB-70DPW*, Catalog No. D10202（3）, 2012-06. Printed in Japan, 2012.

[2] F. Awaja and D. Pavel, “Injection stretch blow moulding process of reactive extruded recycled PET and virgin PET blends,” *European Polymer Journal*, vol. 41, no. 11, pp. 2614–2634, 2005.

[3] M. C. Azhari and E. R. Pribadi, “Analisis Faktor Penyebab Kegagalan Produk Box Mapela Hasil Mesin Injeksi Plastik,” *Jurnal Online Sekolah Tinggi Teknologi Mandala*, vol. 15, no. 1, pp. 27–39, 2020.

[4] B. Demirel, “Optimisation of mould surface temperature and bottle residence time in mould for the carbonated soft drink PET containers,” *Polymer Testing*, vol. 60, pp. 220–228, 2017, doi: 10.1016/j.polymertesting.2017.02.016.

[5] Diego, “Simulation of an Injection Process Using a CAE Tool: Assessment of Operational Conditions and

Mold Design on the Process Efficiency," *Materials Research*, pp. 1–16, 2018.
[6] B. Y. Elapri, "Analisis Kualitas Produk Botol 30ml Dengan Parameter Temperatur Pada Mesin Injection Molding Model Blow," Doctoral Dissertation, Universitas Medan Area, 2023.
[7] N. Iskandar and F. R. Vendiza, "Analisis Cacat Short Shot Dalam Proses Injection Molding Pada Komponen Shroud Fan," in *Prosiding Seminar Sains Nasional dan Teknologi*, vol. 1, no. 1, Aug. 2019.
[8] M. K. Hamdi, "Penyebab Preform Bergelombang Dan Pengaruhnya Terhadap Botol Di Pt Jayatama Selaras, Bogor, Jawa Barat," Doctoral Dissertation, Politeknik ATK, 2023.

LOGIC
Journal of Engineering Design and Technology
Vol. 24 No.3 November 2024; p. 129 - 134

p-ISSN : 1412-114X
e-ISSN : 2580-5649
http://ojs2.pnb.ac.id/index.php/LOGIC

CHARACTERIZATION OF MUNICIPAL SOLID WASTE AS AN ENERGY SOURCE IN THE GASIFICATION PROCESS

I Wayan Temaja[1,3], I Nyoman Suprapta Winaya[2], I Ketut Gede Wirawan[2], Made Sucipta[2], I Putu Angga Yuda Pratama[2]

1) Doctor of Engineering Science of Study Faculty of Engineering, Udayana University
2) Mechanical Engineering Study Program, Faculty of Engineering, Udayana University
3) Mechanical Engineering Department, Bali State of Polytechnic

Correponding email [1] : wayantemaja@pnb.ac.id

Abstract. Municipal solid waste (MSW) poses significant environmental challenges if not managed effectively. The composition and quantity of MSW are closely linked to the socioeconomic structure of a given area. This study aimed to assess the feasibility of utilizing raw materials from Denpasar's MSW for gasification processes. Samples were collected, segregated, processed, and dried for analysis. Various physical and chemical properties were examined, including moisture content, volatility, fixed carbon, elemental composition, and calorific value. Proximate analysis on dry base sample revealed that the MSW contained 12.45% moisture, 54.68% volatile matter, 13.05% fixed carbon, and 19.82% ash. Ultimate analysis showed the following elemental composition: 64.46% C, 11.5% H, 18.3% O, 0.5% N, and 0.05% S, with a calorific value of 11.99 MJ/kg. Based on these findings, the implementation of a waste-to-energy program utilizing gasification processes for waste management is recommended.

Keywords: Municipal Solid Waste, Proximate Analysis, Ultimate Analysis, Gasification.

1. INTRODUCTION

The rapid growth in population and urbanization, coupled with increased industrial development, has led to a surge in global energy demand [1]. The continuous reliance on fossil fuels to meet these energy requirements has been proven to cause significant environmental damage [2]. The combustion of fossil fuels, primarily composed of hydrocarbons, releases CO2 and contributes to the rise in greenhouse gas emissions [3]. This greenhouse effect is a major driver of climate change, resulting in global warming. Consequences of rising global temperatures include crop failures and health issues related to heat waves [4]. Moreover, the current rate of fossil fuel extraction to meet global demand is expected to deplete reserves within this century [5]. These pressing concerns have spurred the development of sustainable, renewable energy sources, including the utilization of waste as an environmentally friendly alternative.

Municipal solid waste (MSW) has emerged as a critical issue due to increasing population and consumption patterns [6]. Generated from various human activities in residential, agricultural, and industrial sectors, MSW can lead to severe environmental problems if not managed effectively. Global MSW production reached 2.01 billion tons in 2016 and is projected to escalate to 2.59 billion tons by 2030 and 3.40 billion tons by 2050 [7]. The composition of MSW varies significantly based on the economic status of communities. Middle- and low-income areas typically produce more organic waste, including food scraps, plant materials, and agricultural residues that are biodegradable. In contrast, high-income regions generate a larger proportion of recyclable waste such as paper, glass, plastic, and metal [8]. Despite concerted efforts to reduce, reuse, and recycle materials, a substantial amount of waste still requires disposal in landfills [9]. However, the continued reliance on landfills presents limitations and can lead to new challenges, including odor issues and health risks [10]. Therefore, effective waste management necessitates well-designed handling programs and infrastructure to mitigate negative impacts on the environment

and public health. As the search for viable alternatives to fossil fuels intensifies, waste has emerged as a promising renewable energy source. The large and consistent volume of waste generated can potentially replace traditional energy sources. Various fuels, including syngas, methane, hydrogen, bio-oil, and biodiesel, can be derived from different waste treatment technologies. Thermochemical and biochemical processes are widely employed to convert waste into energy [11]. Gasification, a thermochemical process, offers a more environmentally friendly approach to waste management. This technique converts MSW components into useful gases such as methane (CH4), hydrogen (H2), and carbon monoxide (CO) for use as fuel [12]. The gasification process involves several stages: drying the biomass to remove water, pyrolysis to separate biomass components, partial oxidation with limited oxygen supply to generate heat, and reduction to produce syngas - a mixture of CO, H2, and CH4.

MSW is inherently heterogeneous, with its calorific value fluctuating based on the conditions of the source area. Utilizing it as a feedstock for the gasification process presents a promising solution to both mitigate energy shortages and address the challenges posed by MSW accumulation [13]. This study aims to examine the composition of MSW in Denpasar to assess its feasibility as a feedstock for the gasification process, potentially paving the way for more sustainable waste management and energy production practices.

2. METHODS

The testing procedure begins with sample preparation, as shown in Figure 1. Sample collection starts with pinpointing the source location in the Denpasar area. The city's dense population and relatively strong economic development have made waste management a pressing issue for the government. MSW, specifically household waste, is transported from various sources to temporary facilities for collection. The diverse composition of municipal solid waste (MSW), characterized by non-flammable materials and high moisture content, requires a meticulous selection process. This ensures that the MSW utilized in testing and subsequent applications is suitable. Effectively addressing this challenge entails sourcing MSW from trustworthy providers. The initial preparation involves homogenizing the raw materials through manual sorting to segregate non-combustible materials like stone, metal, and glass. Organic components are then chopped and sifted to achieve a consistent grain size. For the sample to be used, a sifting test is conducted using a mesh sieve with a size of 40 – 60 mesh to obtain particles ranging from 0.2 to 0.3 mm.

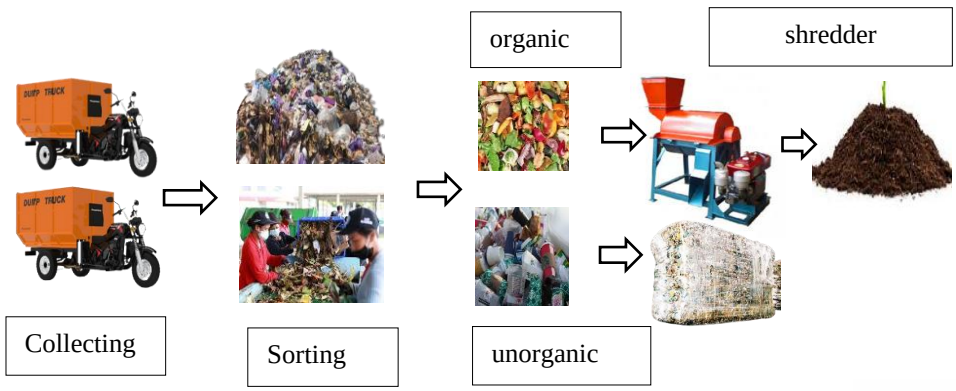

Figure 1. Collecting and preparing MSW procedure

The testing phases conducted include proximate analysis, ultimate analysis, and calorific value testing. These tests are carried out at the NRCE Lab, located at the Faculty of Engineering, Udayana University. Proximate analysis is used to determine the concentration of constituents such as moisture, ash, fixed carbon, and volatile matter in municipal waste fuel. The ASTM D7582 BIOMASS technique is employed, utilizing a test apparatus of type LECO TGA 701. The proximate testing stage begins with a drying procedure to find out the moisture content of the Msw. This involves weighing the sample, approximately one gram, and drying it at 105°C until its weight remains constant, with the difference in weight indicating the moisture content. The sample is then heated to roughly 950°C for seven minutes in an oxygen-free environment to conduct the volatile test. The remaining weight after heating indicates the non-volatile material. To quantify the ash level, the sample is heated in a furnace to 750°C until all organic elements burn, leaving only residues. The weight of the residual ash represents the ash content. Once the moisture content is reduced, the remaining portion of the material comprises volatile matter, while the ash represents fixed carbon.

To analyze the C, H, N, S, and O content in MSW samples, the ultimate test was conducted using the LECO CHN628 instrument, which involved multiple primary phases. To ensure uniformity, the sample is initially prepared, then dried until it attains a constant humidity level, and finally, it is pulverized into a fine powder. The

sample is weighed using an analytical balance to achieve the required 0.5 grams. The LECO CHN628 appliance utilizes two-stage combustion to reach high temperatures of up to 1050 °C while operating in a pure oxygen atmosphere. The combustion gases (CO_2, H_2O, and NOx) are measured with an infrared or conductivity thermal detector, eliminating the requirement for chromatographic separation and allowing for quick and accurate analysis through aliquot dosing and combustion gas handling devices. Processing the data retrieved from the detector yields the weight percentage of each element in the sample.

The bomb calorimeter test was conducted to determine the calorific value of MSW fuel using the LECO Oxygen Bomb Calorimeter. The test involved conditioning dry samples into fine powders, compacting a 1-gram sample, and placing it on a nickel cup in the bomb calorimeter filled with oxygen at a density of 30 Psi, which was then submerged in water. The sample was ignited using an incendiary wire connected to the bomb terminal, initiating combustion in a pure oxygen atmosphere. The heat generated by the combustion was absorbed by the water surrounding the bomb. The increase in water temperature in the calorimeter was measured using a high-resolution digital thermometer. This temperature increase was then used as a reference for calculating the calorific value of the MSW sample.

3. RESULTS AND DISCUSSION

3.1 Proximate analysis

The proximate analysis results of the MSW sample are presented in Figure 2. The result obtained the composition of moisture, volatile materials, ash, and fixed carbon components. Each component has an impact on the quality of syngas produced in the gasification process [14]. Since MSW varies in composition, the moisture content, ash, volatile material content, and elemental compositions will differ accordingly. The moisture content was found to be 12.45% (dry base measurement). The low moisture content percentage is attributed to the sample preparation process, which involved preliminary selection and drying of the samples, leading to a reduction in their moisture content. Moisture plays a critical role in the gasification process of MSW and can significantly impact the system's efficiency, energy output, and overall performance [15]. During the gasification process, the production of H_2O in the reactor increases, leading to the water-gas shift reaction ($CO + H_2O \rightarrow CO_2 + H_2$) and the steam reform process, resulting in higher H_2 and CO_2 content. However, this process requires heat, which can inhibit and lower gasification temperature. Dilution of H_2, CO, and CH_4 concentrations can also reduce the calorific value and energy potential of syngas, ultimately decreasing the overall efficiency of the gasification process. The water content test data indicate that MSW can be used as a raw material for gasification processing.

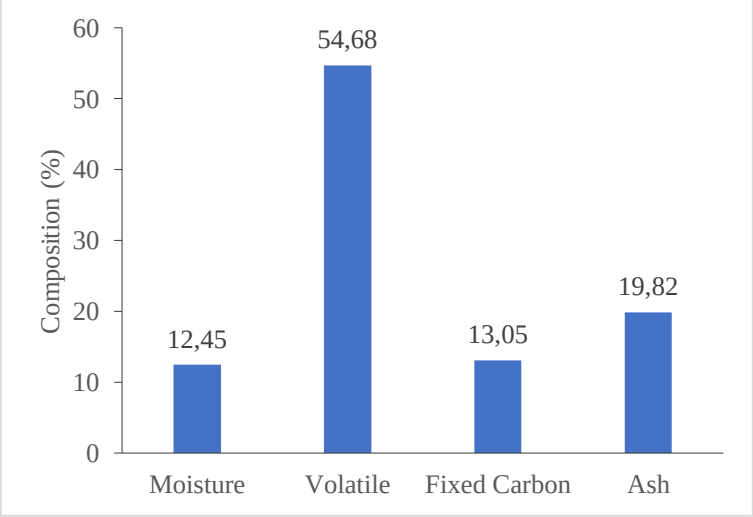

Figure 2. Proximate testing of MSW

The volatile matter of the fuel is crucial in gasification. The high volatile composition indicates the high biomass content of MSW. It vaporizes into gases like H_2, CO, CO_2, CH_4, and hydrocarbons when heated without combustion. Higher volatile content enhances syngas production, especially H_2, and CO, even at lower temperatures during pyrolysis [16]. However, excessive volatility can increase tar formation, complicating the process and requiring additional cleaning. Managing volatile matter is essential to maximize syngas output while minimizing tar-related issues. Ash is the non-combustible residue left after MSW is gasified, made up of minerals like silica, alumina, calcium, and metal oxides. Some ash components, like alkali metals, can catalyze gasification reactions, boosting H_2 and CO production. However, high ash content absorbs heat, lowering gasification

temperatures and reducing H_2 and CO output, while increasing CO_2 and CH_4 levels [17]. Additionally, low-melting-point ash can cause tar formation, disrupting the gasification process. High ash content also requires more energy to maintain temperature, reducing syngas quality and efficiency. The results of the bomb calorimeter test indicated that the MSW sample had a calorific value of 11.99 MJ/kg. This high value suggests that MSW contains a significant amount of flammable materials. This finding aligns with Mukherjee's research [18], which states that the calorific value of MSW typically ranges from 11 MJ/kg to 12 MJ/kg. This calorific value is considered suitable for fuel in the gasification process, which can generate syngas. These syngas can then be utilized as a direct energy source or converted into other fuels.

3.2 Ultimate analysis

The ultimate analysis in Figure 3 provides the percentage of C, H, N, S, and O in the municipal waste sample. The findings show that C, O, and H are the main elements of MSW. C, O, and H in MSW, directly affect syngas production, energy output, and gasification efficiency [19]. N is an element that produces harmful gases like ammonia (NH_3) and nitrogen oxides (NOx). N can dilute the syngas and reduce the quality of the resulting gas. S contributes to the formation of hydrogen sulfide (H_2S) and sulfur dioxide (SO_2). These sulfur compounds are corrosive and toxic, necessitating their removal from the syngas to prevent damage to downstream equipment and reduce environmental impact.

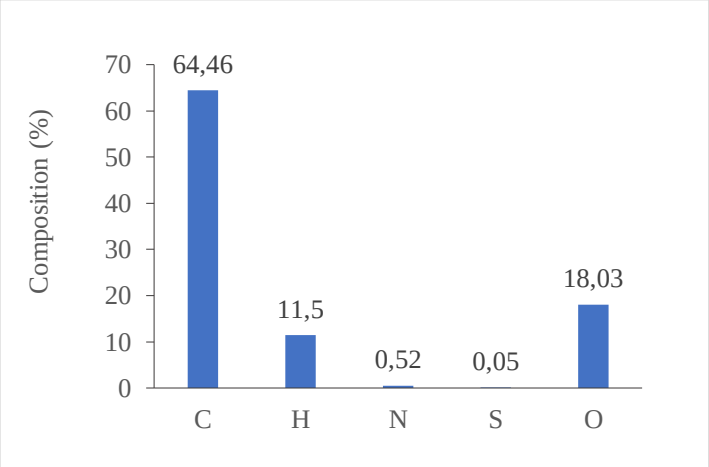

Figure 3. Ultimate testing of MSW

C plays a pivotal role in MSW as it influences the gasification process, directly affecting syngas production, energy output, and gasification efficiency [20]. The exothermic oxidation of carbon ($C + O_2 \rightarrow CO$) helps to sustain the temperature of gasification, thereby promoting endothermic reactions such as the Boudouard reaction and the water-gas reaction. With limited oxygen or air, C is oxidized into CO. In the Boudouard reaction, C reacts with CO_2 to produce CO. In contrast, in the water-gas reaction, C reacts with H_2O to yield H_2 and CO. The concentrations of CO and H_2 have an impact on the calorific value of produced syngas. MSW containing a high C content tends to generate syngas with a higher calorific value, thereby enhancing the overall gasification efficiency. The reaction is :

Oxidation $\quad C + \frac{1}{2}O \rightarrow CO$ (1)

Boudouard reaction $\quad C + CO_2 \rightarrow 2CO$ (2)

Water-gas reaction $\quad C + H_2O \rightarrow CO + H_2$ (3)

The O content in MSW significantly affects combustion and oxidation reactions during gasification. A higher O content in MSW can also influence the stoichiometry of the gasification process, producing CO_2 and H_2O [21]. This has the potential to reduce the calorific value of syngas and the efficiency of syngas production. Conversely, H enhances syngas' calorific value since H_2 is a very energetic fuel component. A higher H content in MSW generally leads to a higher concentration of H_2 in the syngas, which enhances its overall quality as a fuel. Several tests conducted in various locations, including Osogbo, Chattogram City, and Morocco [22,23,24], have shown that the composition of the elements from the proximate and ultimate analyses yielded comparable results. Additionally, when compared to Cassius' research [25], which reported a low heating value of 4.6 MJ/kg, the findings from this test indicate that the material is suitable for use as raw material in the gasification process

.

4. CONCLUSION

The proximate and ultimate analyses of MSW indicate that elements such as volatiles and carbon, present in high percentages, have a positive impact on syngas production and calorific value. Moreover, the composition of components such as moisture content, ash, hydrogen, and oxygen is sufficient to support the gasification process. Elements like nitrogen and sulfur, which can potentially reduce the quality of syngas and lower the calorific value, are present only in small percentages. It is important to note that the sample preparation process, including sorting and drying, significantly affects the composition of these elements. Based on these findings, MSW from the sampled source is recommended for use as a raw material in the gasification process.

5. ACKNOWLEDGEMENT

This research is supported by the New Renewable & Conversion Energy (NRCE) research group of Udayana University. The authors are grateful for the support of staff and students of the Faculty of Engineering, Udayana University, as well as the cooperation of the local government and waste management authorities.

6. REFERENCES

[1] I. F. U. Muzayanah, H. H. Lean, D. Hartono, K. D. Indraswari, and R. J. H. Partama, "Population density and energy consumption: A study in Indonesian provinces," vol. 8, no. 9, 2022.
[2] R. Ali, K. Bakhsh, M. A. J. S. C. Yasin, and Society, "Impact of urbanization on CO2 emissions in emerging economy: evidence from Pakistan," vol. 48, p. 101553, 2019.
[3] A. N. Wafiq, S. J. J. E. Suryanto, and S. Pembangunan, "The Impact of Population Density and Economic Growth on Environmental Quality: Study in Indonesia," vol. 22, no. 2, pp. 301-312, 2021.
[4] A. Mikhaylov, N. Moiseev, K. Aleshin, T. J. E. Burkhardt, and S. Issues, "Global climate change and greenhouse effect," vol. 7, no. 4, p. 2897, 2020.
[5] C. Day and G. J. E. M. Day, "Climate change, fossil fuel prices and depletion: The rationale for a falling export tax," vol. 63, pp. 153-160, 2017.
[6] Y.-C. J. W. m. Chen, "Effects of urbanization on municipal solid waste composition," vol. 79, pp. 828-836, 2018.
[7] S. Kaza, L. Yao, P. Bhada-Tata, and F. Van Woerden, What a waste 2.0: a global snapshot of solid waste management to 2050. World Bank Publications, 2018.
[8] K. Kala and N. B. J. M. o. E. Q. A. I. J. Bolia, "Effects of socio-economic factors on quantity and type of municipal solid waste," vol. 31, no. 4, pp. 877-894, 2020.
[9] I. T. J. E. J. o. E. Osazee and E. Sciences, "Landfill in a sustainable waste disposal," vol. 2, no. 4, pp. 67-74, 2021.
[10] A. Iravanian and S. O. Ravari, "Types of contamination in landfills and effects on the environment: A review study," in IOP conference series: Earth and environmental science, 2020, vol. 614, no. 1, p. 012083: IOP Publishing.
[11] R. Nandhini, D. Berslin, B. Sivaprakash, N. Rajamohan, and D.-V. N. J. E. C. L. Vo, "Thermochemical conversion of municipal solid waste into energy and hydrogen: a review," vol. 20, no. 3, pp. 1645-1669, 2022.
[12] P. Basu, Biomass gasification, pyrolysis and torrefaction: practical design and theory. Academic press, 2018.
[13] P. Behrend, B. J. S. P. Krishnamoorthy, and Consumption, "Considerations for waste gasification as an alternative to landfilling in Washington state using decision analysis and optimization," vol. 12, pp. 170-179, 2017.
[14] Y. Gao et al., "Syngas Production from Biomass Gasification: Influences of Feedstock Properties, Reactor Type, and Reaction Parameters," ACS Omega, vol. 8, no. 35, pp. 31620-31631, 2023/09/05 2023.
[15] I. L. Motta, N. T. Miranda, n. Maciel, and R. Filho, "Biomass gasification in fluidized beds: A review of biomass moisture content and operating pressure effects," Renewable Sustainable Energy Rev., vol. 94, p. 998, 2018.
[16] M. Al-Zareer, I. Dincer, and M. A. J. J. o. E. R. T. Rosen, "Influence of selected gasification parameters on syngas composition from biomass gasification," vol. 140, no. 4, p. 041803, 2018.
[17] A. S. Al-Rahbi and P. T. J. A. E. Williams, "Hydrogen-rich syngas production and tar removal from biomass gasification using sacrificial tyre pyrolysis char," vol. 190, pp. 501-509, 2017.
[18] Mukherjee, Chandrani, J. Denney, Eric G. Mbonimpa, J. Slagley, and R. Bhowmik. "A review on municipal solid waste-to-energy trends in the USA." Renewable and Sustainable Energy Reviews 119 (2020): 109512.
[19] Y. Zhang et al., "A review on biomass gasification: Effect of main parameters on char generation and reaction," vol. 34, no. 11, pp. 13438-13455, 2020.
[20] B. Dai et al., "Effect of the composition of biomass on the quality of syngas produced from thermochemical conversion based on thermochemical data prediction," vol. 33, no. 6, pp. 5253-5262, 2019.
[21] L. Wang, X. Du, J. Chen, and Z. J. R. E. Wu, "Numerical study on characteristics of biomass oxygen enriched gasification in the new gasifier on an experimental basis," vol. 179, pp. 815-827, 2021.

[22] B. Adeboye, M. Idris, W. Adedeji, A. Adefajo, T. Oyewusi, and A. J. C. W. S. Adelekun, "Characterization and energy potential of municipal solid waste in Osogbo metropolis," vol. 2, p. 100020, 2022..
[23] A. M. M. Hassan et al., "Characterization of municipal solid waste for effective utilization as an alternative source for clean energy production," vol. 16, no. 4, p. 100683, 2023.
[24] O. Bourguig, A. Ramos, K. Bouziane, M. Asbik, E. Monteiro, and A. J. E. R. Rouboa, "Performance assessment of the co-gasification for sustainable management of municipal solid waste: Moroccan Case," vol. 8, pp. 1530-1540, 2022..
[25] C. R. Ferreira et al., "Gasification of municipal refuse-derived fuel as an alternative to waste disposal: Process efficiency and thermochemical analysis," vol. 149, pp. 885-893, 2021.

LOGIC
Journal of Engineering Design and Technology
Vol. 24 No.3 November 2024; p. 135 - 140

p-ISSN : 1412-114X
e-ISSN : 2580-5649
http://ojs2.pnb.ac.id/index.php/LOGIC

DESIGN OF A GROUTLESS CLEAR COFFEE MACHINE USING DISTILLATION METHOD

Adi Pratama Putra [1], Megandhi Gusti Wardhana [2], Charis Fathul Hadi [3]

1) Mechanical Engineering Study Program, Faculty of Engineering, Banyuwangi PGRI University, Banyuwangi, Indonesia
2) Agricultural Product Processing Study Program, Faculty of Agriculture, Banyuwangi PGRI University, Banyuwangi, Indonesia
3) Electrical Engineering Study Program, Faculty of Engineering, Banyuwangi PGRI University, Banyuwangi, Indonesia

Corresponding email [1] : tama.adie@yahoo.com

Abstract. Coffee is a plantation commodity that is made into a drink as one of the products that is popular with the public. Many coffee drink innovations have been made, one of which is a clear coffee drink without dregs. The process of making clear coffee can be done by the distillation method, namely the process of condensing the steam produced by a mixture of coffee powder and water. This study aims to obtain the design results of a clear coffee machine without dregs using the distillation method. The design is carried out based on the results of a patented study on making clear coffee. The coffee machine is made with a heating tube for a mixture of ground coffee and water, a steam collector tube and a distillation tube. The design results obtained a heating tube with a diameter of 25 cm and a height of 27 cm for a process capacity of 13.25 liters. Heating is performed using an LPG-fueled heater. The distillation process is carried out by cooling the water using a 15 watt aerator pump. The trial was carried out by processing 500 grams of fine coffee powder mixed with 2000 ml of water. The trial results obtained 500 ml of clear coffee with an average process time of ± 25 minutes.

Keywords: Design, Machine, Clear Coffee, Distillation.

1. INTRODUCTION

Coffee is one of the plantation commodities that plays a significant role in economic activities in Indonesia. Coffee production in 2020 was 762.38 thousand tons, in 2021 it was 786.19 thousand tons and in 2022 it was 774.96 thousand tons [1]. Indonesian coffee has different sizes, flavors, and characteristics according to the area of origin of the coffee so that the Indonesian nation is rich in coffee flavors [2]. The potential of coffee products is part of the utilization of appropriate technology, especially for mechanical technology in its processing. The application of appropriate technology has been widely used for post-harvest processing of coffee. This includes coffee bean sorting machines [3], coffee skin peelers [4][5][6], coffee bean washing machines [5], roasting machines [7][8][9][10], grinding machines [2][8][11], coffee powder sieving machines [12] and coffee powder packaging machines [13].

The majority of Indonesians like coffee drinks as a refreshing beverage enjoyed during leisure time [14]. Coffee is packaged with a distinctive taste and aroma so that connoisseurs always want to taste it again. As a result, coffee consumption in Indonesia increases by 6-8 percent per year [15]. Coffee drink products have been innovated, including palm sugar milk coffee products [16] and wine coffee [17]. Innovation has also been made for coffee making machines or devices. These innovations include the design of an automatic coffee maker using a conveyor [18], the design of an automatic coffee maker based on Arduino Uno with Android control [15], the design of a coffee water maker with a robotic system [14], the manufacture of an espresso coffee machine using a pneumatic system [19], the design of an automatic milk coffee machine based on Arduino [20].

Another innovation in coffee beverage products is clear coffee without dregs. This innovation was obtained from research results where the appropriate formulation was carried out with a roasting temperature of 195°C and a

ratio of ground coffee formulation to spring water of 10 g: 50 ml [21]. Characterization of clear coffee in testing pH levels, protein levels, water content, ash content, fat content, and caffeine levels resulted in the dark roasting treatment (195°C - 200°C) having the highest percentage value with low caffeine levels and the roasting temperature treatment of 195°C - 200°C had the highest level of preference [22].

This clear coffee product has been patented [23]. The manufacture of clear coffee uses the principle of condensation of coffee vapor or by the distillation method. The manufacturing process requires appropriate equipment or machines. For this reason, research is needed that aims to obtain the design results of a clear coffee machine without dregs using the distillation method.

2. METHODS

The design of the clear coffee machine refers to the steam distillation process of coffee. Clear coffee has been tested organoleptically and proximately for the characteristics of clear coffee with research that has been done. The patent for clear coffee is a series of processes for further production processes using the appropriate machine. The clear coffee machine is designed with the scheme in Figure 1.

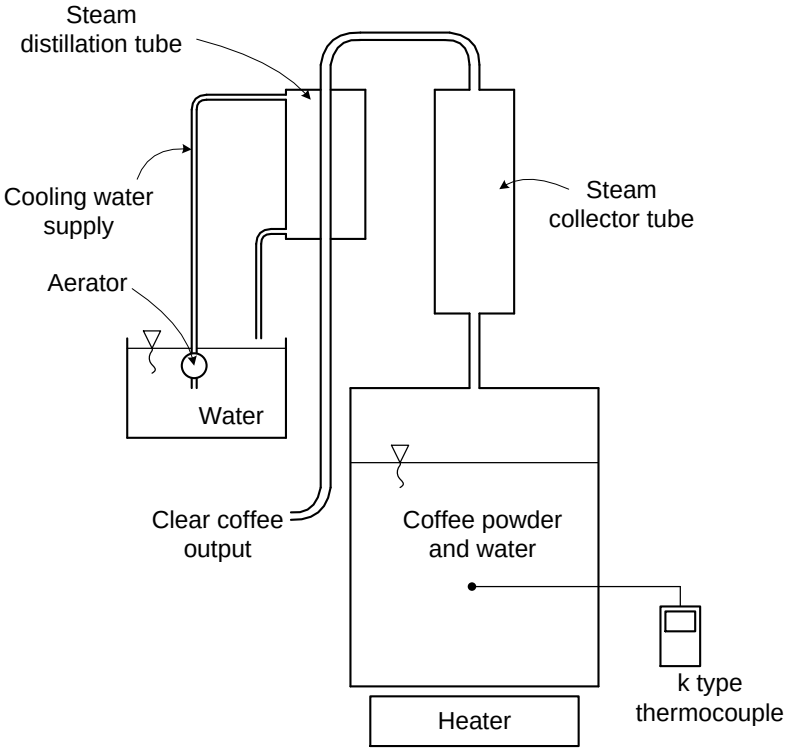

Figure 1. Schematic of clear coffee machine

Figure 1 shows a tube filled with finely ground and roasted coffee powder. Water is mixed into the tube and heated at the bottom of the tube. After a period of heating, coffee steam is produced. The pressurized coffee steam will move up into the steam collection tube. The collected coffee steam then flows into the distillation tube. Condensation occurs as cold water flows into the distillation tube, functioning like a heat exchanger. Cold water is circulated with an aerator or submersible pump. The coffee steam that interacts with the cold water will condense so that it drips into clear coffee liquid.

The design of the clear coffee machine was carried out with the design, manufacturing and testing stages of the tool. The machine trial was carried out by processing 500 grams of coffee powder mixed with 2000 ml of water. Heating was carried out using an LPG stove. The trial was carried out to obtain 500 ml of clear coffee. In the trial, data was recorded on the process time to produce 500 ml of clear coffee. Time measurements were taken using a stopwatch. Time measurements were taken after the water temperature in the tube reached 90°C where at this temperature, coffee steam production began. This temperature was monitored using a type K thermocouple. The thermocouple was submerged in the center of the tube. The trial was carried out five times.

3. RESULTS AND DISCUSSION

3.1. Design Result

The heating tube has a diameter of 25 cm and a height of 27 cm. With this size, the volume of the tube is 13,25 litre. The steam collector tube is designed with a diameter of 6 cm and a height of 30 cm so that the steam collector tube has a volume capacity of 0.85 liters. The distillation tube is made with a diameter of 6 cm and a height of 18 cm. An aerator pump with a power of 15 watts is used to supply cold water. For the distillation process, coffee steam is flowed through a copper tube positioned on the axis of the distillation tube. The copper pipe used is 20 mm in diameter and 2 mm thick. Copper is chosen because of its relatively good heat conductor properties so that it can optimize heat exchange between coffee steam and cooling water. All tubes are made of stainless steel. This is because the process of making clear coffee must not be contaminated with corrosion caused by the equipment material. While other accessories such as water hoses use plastic materials.

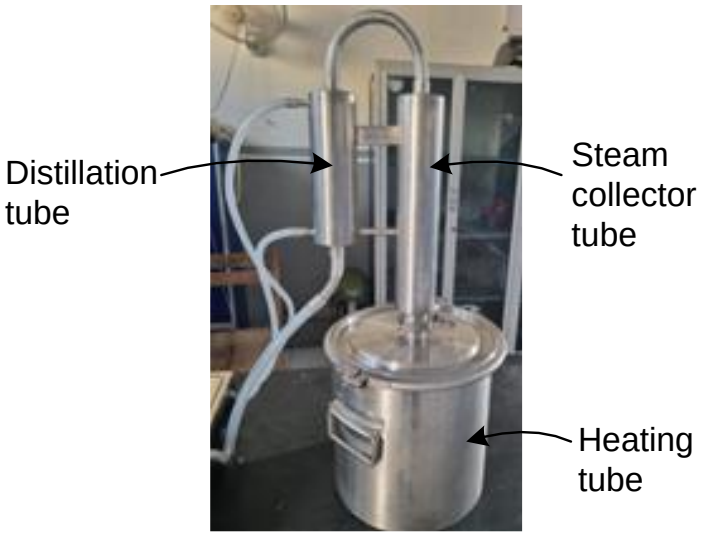

Figure 2. Results of the clear coffee machine design

3.2. Trial Result

The trial results are shown in the following table 1.

Table 1. Trial results

Number of trial	Processing time (second)	Processing time (minute)
1	1524,32	25,41
2	1511,74	25,20
3	1498,06	24,97
4	1492,13	24,87
5	1539,84	25,66
Average	1513,22	25,22

Table 1 shows that the average time required to produce 500 ml of clear coffee is 25.22 minutes. The photo of the clear coffee product is shown in Figure 3. The product photo shows that the coffee produced is relatively clear and without grout.

Figure 3. Photo of the product from the trial

The main target of this clear coffee machine design is that the equipment that is designed can produce clear coffee. This is done as a development of research results that have been carried out in the laboratory. The main drawback of this equipment is the relatively long process time so that further innovation needs to be done to optimize the process time.

3.3. Comparison With Similar Designs

In general, the design of the clear coffee machine has been able to produce the expected product. The energy requirements to produce 500 ml of clear coffee are:

a. LPG fuel.
   This fuel is used to heat the mixture of coffee powder and water. Heating is carried out for ± 26 minutes according to the test results. Based on the research results, LPG consumption for 10 minutes of combustion requires ± 0.135 kg of fuel [24]. So the consumption of LPG fuel for this heating is ± 0.3375 kg. The propane compound in LPG has a heating value of 50.35 MJ/kg or equal to 50350 kJ/kg so that the use of 0.3375 kg is equivalent to 16,993.13 kJ.
b. Electrical energy.
   Electrical energy is used to drive the aerator pump in the distillation process. The pump used has a power of 15 watts. The process time for 25 minutes requires 36 watts of electrical energy. This energy quantity is equivalent to 36 J/s.

Automatic coffee maker based on robotics or Arduino control uses a 12 Volt power supply as a source of electrical energy for its supporting components, including sensors, solenoids, servo motors and others. Assuming there are 5 supporting components, an electric current of 2 Ampere and an average process time of 5 seconds, the energy consumption is 120 watts per second or 120 J/s. Automatic coffee maker using a conveyor also requires similar supporting components so that its energy requirements are relatively the same. A coffee maker with a pneumatic principle requires a compressor as a source of compressed air. Assuming a compressor power of 0.25 HP and a process time of 5 seconds, the energy consumption is 932.125 J/s.

Table 2
Comparison of energy consumption with previous research

Design Topic	System	Energy Consumption
Automatic coffee machine	Robotic or Arduino control	120 J/s
Automatic coffee machine	Pneumatic	932,125 J/s
Clear coffee machine	Distilation	17,029.13 kJ/s

Table 2 shows that the energy consumption of clear coffee machines is very large compared to automatic coffee machines from previous studies. This difference occurs because making clear coffee requires LPG as a heating fuel. The large amount of energy required is a consequence of the heating value of the propane compound in LPG. On the other hand, automatic coffee machines are designed for coffee drinks that are consumed immediately so they only require hot water and stirring. The resulting drink is not a type of drink that is durable to store. In addition, automatic coffee machines produce coffee drinks with residue or dregs so that they are very different from clear coffee products. Water heating in the design of previous studies was not discussed explicitly.

3.4. Further Innovation Opportunities

The time required to produce 500 ml of clear coffee is an average of ± 25 minutes, which means 0.33 ml/sec is produced. The temperature of the heating tube must be maintained at more than 90ºC so that steam production can be sustainable. In this way, the distillation process can run optimally so that it will produce optimal products. Efforts to improve machine performance can be done by:

1. Increasing the amount of coffee steam production by increasing the diameter of the tube. A larger tube diameter is equipped with even heating so that more coffee water mixture is evaporated.
2. Optimizing the distillation process by flowing water at a lower temperature. Lower temperatures will accelerate the steam condensation process. The distillation tube device can also be equipped with barrier partitions to create vortices that will improve heat exchange performance.

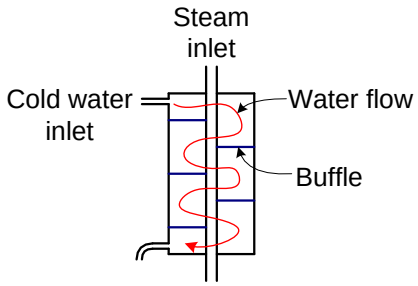

Figure 4. Schematic of adding a barrier partition in the distillation tube

Figure 4 shows a schematic of a distillation tube with the addition of barrier partitions. This innovation refers to the heat transfer model of a heat exchanger. The partitions will cause the water flow to meander so that the flow path becomes longer. The length of the path will provide more opportunities for the cooling water to exchange heat with the coffee steam. This increase in heat exchange performance will result in a more optimal condensation process.

The design results of the clear coffee machine have been tested well. For application on a production scale, it still requires feasibility in terms of production costs. Economic analysis is still needed so that the application of this clear coffee machine has the potential to be an alternative variant of the coffee drink business.

4. CONCLUSION

The design of a clear coffee machine without grounds using the distillation method has been carried out. The machine can produce 500 ml of clear coffee in about 25 minutes. Optimization of production can be done by changing the dimensions of the heating tube and distillation tube.

5. ACKNOWLEDGEMENT

This publication article is an output of a series of grant funding activities Program Dana Padanan Direktorat Riset, Teknologi, dan Pengabdian Kepada Masyarakat Direktorat Jenderal Pendidikan Tinggi, Riset, dan Teknologi Kementerian Pendidikan, Kebudayaan, Riset, dan Teknologi, for fiscal year 2024.

6. REFERENCES

[1] Sub Direktorat Statistik Tanaman Perkebunan, *Statistik Kopi Indonesia Indonesian Coffee Statistics 2022*. Badan Pusat Statistik/BPS-Statistics Indonesia, 2023.

[2] E. Marpaung and R. P. Hutasoit, “Rancang Bangun Mesin Penggiling Kopi dari Biji Kopi Menjadi Bubuk Kopi Dengan Kapasitas 50 Kg/ Jam,” *J. Teknol. Mesin UDA*, vol. 2, no. 1, pp. 115–119, 2021.

[3] N. Aprini, Heriansyah, P. Maharani, and L. Y. Syah, “Penerapan Teknologi Tepat Guna pada UKM Pengolahan Kopi di Kota Pagar Alam,” *J. Pengabdi. Masy. Tri Pamas*, vol. 3, no. 1, pp. 50–65, 2021.

[4] Z. Nurisna and S. Anggoro, “Peningkatan Kualitas Produk Biji Kopi Robusta di Desa Nglinggo Barat , Kelurahan Pagerharjo , Kecamatan Samigaluh, Kabupaten Kulon Progo,” in *Seminar Nasional Abdimas II 2019, Sinergi dan Strategi Akademisi, Business dan Government (ABG) Dalam Mewujudkan Pemberdayaan*

Masyarakat yang Berkemajuan di Era Industri 4.0, 2019, pp. 1311–1319.
[5] I. Mawardi, Hanif, Zaini, and Z. Abidin, "Penerapan Teknologi Tepat Guna Pascapanen Dalam Upaya Peningkatan Produktifitas Petani Kopi di Kabupaten Bener Meriah," *Caradde J. Pengabdi. Kpd. Masy.*, vol. 1, no. 2, pp. 205–213, 2019, doi: https://doi.org/10.31960/caradde.v1i2.56.
[6] A. Z. Siregar, Yunilas, and Irsal, "Pengolahan Kopi Tepat Guna Mendukung Pertanian di Desa Telagah, Sei Bingei, Langkat," *Charity, J. Pengabdi. Masy.*, vol. 05, no. 1, pp. 7–18, 2022, doi: https://doi.org/0000-0002-7077-9852/.
[7] I. Kholiq and Y. Probowati, "PKM TTG Kopi Bubuk Untuk Meningkatkan Kapasitas di Benowo Surabaya," in *Prosiding PKM-CSR*, 2019, vol. 2, pp. 340–346.
[8] Amal, E. Syarif, and Uca, "Melalui Penerapan Teknologi Tepat Guna Pengolahan Kopi di Desa Karueng Kabupaten Enrekang Sulawesi Selatan," in *Prosiding Seminar Nasional*, 2019, pp. 1–3.
[9] Pramono, M. A. Habibi, F. I. Kusuma, Sujito, Suprayitno, and S. Azzahra, "Automatic Coffee Bean Roaster Machine to Improve Production Quality and Efficiency for Coffee Business," *Communnity Dev. J.*, vol. 4, no. 3, pp. 6450–6454, 2023.
[10] P. A. Wicaksono, A. Wibawa, B. Santoso, and M. D. Pertanian, "Penerapan Teknologi Tepat Guna Mesin Roasting Kopi pada UKM Kopi Pinanggih," *J. Pasopati*, vol. 5, no. 3, pp. 138–143, 2023.
[11] Solikhin, P. A. Wicaksono, and A. W. B. Santoso, "Teknologi Tepat Guna Mesin Grinder Listrik Sebagai Sarana Peningkatan Produksi Kopi pada UKM Kopi Pinanggih," *J. Pasopati*, vol. 5, no. 2, pp. 73–78, 2023.
[12] V. E. B. Darmawan, A. Larasati, W. Irdianto, F. R. Salsabila, and D. Prastyo, "Penerapan Teknologi Tepat Guna Ergonomics Mesh Strainer Tool Dalam Peningkatan Kualitas dan Kuantitas Produksi Kopi pada UMKM Djapa Coffee Di Kabupaten Malang," *JP2T*, vol. 2, no. 2, pp. 106–111, 2023.
[13] Sujito, M. R. Faiz, Aripriharta, A. A. Hadi, and M. Z. Falah, "Pemanfaatan Teknologi Continuous Band Sealer Guna Meningkatkan Efisiensi Packing UMKM Kopi Wali Desa Toyomarto," *J. Pengabdi. Pendidik. Masy. (JPPM)*, vol. 4, no. 2, pp. 293–298, 2023.
[14] M. F. Alfaridzi and Agustiawan, "Rancang Bangun Mesin Pembuat Air Kopi Dengan Sistem Robotik," in *Seminar Nasional Industri dan Teknologi (SNIT)*, 2020, no. 1, pp. 328–334.
[15] N. Firmawati, G. Farokhi, and W. Wildian, "Rancang Bangun Mesin Pembuat Minuman Kopi Otomatis Berbasis Arduino UNO dengan Kontrol Android," *JITCE (Journal Inf. Technol. Comput. Eng.*, vol. 01, no. 03, pp. 25–29, 2019, doi: https://doi.org/10.25077/jitce.3.01.25-29.2019.
[16] M. F. Lisan *et al.*, "Inovasi Produk Pengolahan Kopi Susu Gula Aren Serta Strategi Pemasaran Dalam Upaya Meningkatkan Perekonomian Masyarakat Desa Sambik Bangkol Lombok Utara," *J. Pengabdi. Magister Pendidik. IPA*, vol. 6, no. 1, pp. 179–184, 2023, doi: https://doi.org/10.29303/jpmpi.v6i1.3247.
[17] W. B. Sunarharum, S. A. Mustaniroh, F. D. Riana, and D. F. Azizah, "Peningkatan Kapabilitas, Dayasaing Dan Teknologi Produksi Kopi Wine Sebagai Produk Unggulan Penyangga Meru Betiri Di Desa Kebonrejo Kec. Kalibaru, Banyuwangi," *J. Innov. Appl. Technol.*, vol. 09, no. 01, pp. 88–94, 2023.
[18] I. N. Rosi, "Rancang bangun alat pembuat minuman kopi otomatis menggunakan konveyor," *J. Ilm. Mikrotek*, vol. 2, no. 4, pp. 35–45, 2017.
[19] M. Elyan, R. Winarso, and R. Wibowo, "Pembuatan Mesin Kopi Espresso Menggunakan Sistem Pneumatik," *J. CRANKSHAFT*, vol. 5, no. 1, pp. 65–72, 2022.
[20] Sujono, R. Sihab, and N. Yaqin, "Design of Automatic Coffee and Milk-Making Machine Based on Arduino," *Saintekbu J. Sci. Technol.*, vol. 15, no. 02, pp. 17–26, 2023.
[21] M. G. Wardhana and M. S. Irwan, "Formulasi Inovatif Pembuatan Kopi Bening Tanpa Ampas (Clear Coffee)," *J. Agrotek Ummat*, vol. 7, no. 1, pp. 12–19, 2020.
[22] M. G. Wardhana and M. S. Irwan, "Analisis Karakteristik Kandungan Kopi Bening (Clear Coffee) Kabupaten Banyuwangi," *Agrotek Ummat*, vol. 7, no. 2, pp. 65–72, 2020.
[23] M. S. I. Hariandi and M. G. Wardhana, "Metode Pembuatan Kopi Bening," A 23F 5/00,A 23N 12/00, 2022.
[24] S. Azzahra, H. Azis, M. T. B. Sitorus, and Pawenary, "Uji Performa Kompor Induksi dan Kompor Gas Terhadap Pemakaian Energi dan Aspek Ekonomisnya," *Energi dan Kelistrikan J. Ilm.*, vol. 12, no. 2, pp. 149–155, 2020, doi: https://doi.org/10.33322/energi.v12i2.1009.

LOGIC
Journal of Engineering Design and Technology
Vol. 24 No.3 November 2024 ; p. 141 - 149

p-ISSN : 1412-114X
e-ISSN : 2580-5649
http://ojs2.pnb.ac.id/index.php/LOGIC

INFLUENCE OF MIG WELDING PROCESS PARAMETERS ON THE STRENGTH OF BIMETAL JOINTS: STUDY OF GAS FLOW RATE AND MACROFRACTURES

Talifatim Machfuroh [1*], Kris Witono [2], Septyana Riskitasari [3], Etik Puspitasari [4]

1,2,3,4) Mechanical Engineering, Malang State Polytechnic, Malang City, Indonesia

Corresponding email [1] : talifatim.machfuroh@polinema.ac.id

Abstract. Bimetal joints are often used in various industries, such as automotive, power generation, electronics, and manufacturing. This is because bimetal joints allow the joining of two types of metal with different properties. Welding two different types of metal can pose its own challenges, such as the difficulty of controlling welding parameters so that the results are optimal for both types of metal, as well as differences in the thermal and mechanical properties of the two metals. This has led to extensive research on bimetal plate connections. Based on this background, this research aims to determine the effect of variations in flow rate and current strength on the tensile strength of robotic welding bimetal welded joints, as well as determine the results of macro photos of fractures resulting from tensile tests for each variation. The research was carried out experimentally where each variation was repeated with data 3 times. Based on the results and discussion, it is known that the optimal gas flow rate in general is 20 l/min, where the tensile strength reaches 353.1442 MPa–455.5458 MPa. At this flow rate, the dominant fracture occurs in the base metal and is ductile, which indicates good plastic deformation. On the other hand, gas flow that is too low or too high causes joint defects and reduces the tensile strength. Meanwhile, other welding parameters, namely variations in welding current, affect tensile strength. At a gas flow of 10 l/min, increasing the current to 180 A produces the highest tensile strength of 449.4357 MPa with ductile fracture characteristics. However, at a current of 120 A there is a significant decrease due to overheating, especially at higher gas flows such as 20 l/min and 30 l/min, which results in brittle fracture in the heat-affected zone (HAZ). The results of this research contribute to the understanding of the influence of welding parameters on the tensile strength and fracture characteristics of bimetallic joints. In addition, this research can be a reference for the development of more efficient and reliable welding processes in various industries, such as automotive, power generation and manufacturing, which require bimetallic joints with optimal quality.

Keywords : Bimetal, Mig, Joint, Welding

1. INTRODUCTION

The modern manufacturing industry continues to develop rapidly along with increasing demand for high quality products and efficient production processes. Welding is one of the most commonly used methods of joining materials in the manufacturing industry [1]. One important application of this technology is bimetal welding, which involves wcombining two types of metal with different physical properties into one unit [2].

Bimetal welding between steel plates and stainless steel has important uses in various industries because it combines high mechanical strength and corrosion resistance [3][4]. In the construction, energy and military industries, bimetallic welding is applied to bridges, power plants, armored vehicles and warships, where it can provide the combination of heat resistance, strength and corrosion resistance required in harsh and extreme environments [5][6]. Apart from that, bimetal is also used to make pipes and other components that require corrosion resistance on one side and high mechanical strength on the other side, such as in oil and gas piping systems, heat exchangers, pressure vessels, and so on [7].

The bimetal welding process has its own challenges, especially in terms of the strength of the resulting joint. Differences in the thermal and physical properties of the two metals being welded can cause discrepancies in the connection, such as cracking or freezing. To overcome this problem, various welding parameters need to be carefully controlled, including the gas flow rate and the electric current used during the welding process.

Shielding gas in MIG welding functions as a protector against dangerous contamination that can cause defects. In addition to these main functions, shielding gases significantly influence the weld shape, weld geometry, layer appearance, metallurgical and mechanical properties, welding speed, metal displacement, arc stability or light and smoke emissions [8]. Setting the gas flow rate affects the environment around the welding arc and the weld results [8]. Bintarto, et al [9] have analyzed the effect of Tungsten Inert Gas (TIG) protective gas flow rate on tensile strength and toughness (shock) in welded joints between galvanized steel and aluminum 5052, using Al-Si 4043 filler. This welding process involves two metals that have different characteristics. Control of the inert gas flow rate is essential to prevent oxidation and produce strong joints. Cai, et al, [10] analyzed the effect of a mixture of argon (Ar) and helium (He) shielding gases on the welding characteristics of the fiber laser-MIG (Metal Inert Gas) hybrid welding method for aluminum alloys. This research focuses on how variations in the proportions of Ar and He in the shielding gas mixture affect welding results, including joint strength, surface quality, as well as the stability and efficiency of the welding process on aluminum alloys. X. Yang, H., et al, [11] and Campana [12] studied the effect of shielding gas flow rate on the welding process in hybrid laser-arc welding and MIG welding methods.

Several studies have been carried out to determine the factors that influence the quality of MIG welded joints, including research conducted by Sarjiyana [13] and Kurniawan [14] in their research on tensile strength in welding. In this research, it was found that there was an influence of voltage and current strength on the tensile strength of welded joints. In their research, Wenny [15] and Roymons [16] also examined the effect of variations in welding electric current on the strength of MIG welding joints. In this research, it was also found that there was a significant influence. Other research related to the influence of gas flow rate has also been studied by Swami [17]. In his research, it was found that the optimum value of tensile strength of 356 N/mm^2 was observed at a welding current of 190 A, a gas flow rate of 15 l/minute, & a gas combination of 50% CO2+50 % Argon. Of the several studies that have been carried out, not many have conducted research on bimetal plate connections. Most joints are made in the same material. Apart from that, the welding carried out still uses manual welding, so the quality of the welding is also determined by operator factors. Bahar et al., 2018 in their research Sukhbir, 2022 [18] observed the impact of MIG welding input variables on hardness and UTS of dissimilar metals mild steel and stainless-steel welded joints. The contribution of gas flow rate was greater than other parameters. Improved UTS of the weldment was achieved at lower welding voltage and higher weld speed. The maximum UTS value was approximately 235 MPa. Zhu et al., 2018 analyzed the influence of preheating on the microstructural behavior of MIG welded 5083 aluminum alloy joints. A large number of equiaxed grains were noticed in the HAZ [19].

On the other hand, research on the strength of bimetallic steel welded joints was carried out by Kris Witono in his research [20] on variations in travel speed and stickout length on the tensile strength of bimetallic steel. In this research, the connection used was a low carbon steel bimetallic connection with stainless steel. It's just that other factors such as current strength and gas flow rate have not been studied further in this research. In bimetallic joining, setting this parameter becomes more critical due to the differences in the thermal characteristics of the two metals being joined. Errors in parameter setting can cause cracks, distortion, or other defects in the joint that can reduce the strength of the joint. Therefore, this study aims to understand how variations in gas flow rate in the MIG welding process affect the strength of bimetal joints and the form of fracture that occurs, as well as to find optimal parameters that can produce joints with the best strength.

2. METHODS

Research methods and stages include: 1) material preparation. The materials used are low carbon steel plates and 304 series stainless steel plates with a thickness of 3 mm. 2) Welding process. After the material is cut, the joining

process is carried out using MIG welding which is operated with varying gas flow rates of 10 l/minute, 20 l/minute, and 30 l/minute. The travel speed was controlled, and currents of 100 A, 120 A, 140 A, 160 A, and 180 A were used. The filler wire used in the welding process is type ER308L with a diameter of 0.8 mm. 3) Tensile testing. Tensile testing is carried out using the ASTM E8M tensile test standard. Each sample was pulled using a tensile testing machine to measure ultimate tensile strength (UTS) and elongation. This test is carried out for each variation of welding speed to obtain data on the effect of travel speed on tensile strength. Each variation was tested three times. 4) Observation of macro photos involves identifying ductile fracture patterns (presence of necking, cup and cone pattern) or brittle fracture. 5) Analysis and discussion. The results of data analysis are prepared in a clear and structured research report.

Figure 1. ASTM E8M standard test specimen

The tensile test results in the form of a stress-strain curve were observed and the test results were compared between sample groups. From this curve, various important parameters such as yield strength, ultimate tensile strength, and fracture strain can be identified. Apart from that, macro and micro photos of the joint results were also observed to understand the fracture characteristics and crack morphology in the joint or material being tested. Data obtained from these observations include the type and pattern of cracks, the location of the initial crack, and the type of failure that occurred (e.g., ductile failure or brittle failure).

3. RESULTS AND DISCUSSION

3.1. Results

a. Effect of varying gas flow rate on welding current 100A

The relationship between variations in gas flow rate and tensile strength at a welding current of 100 A is shown in Figure 2. Based on this graph, the effect of variations in gas flow rate on the tensile strength of bimetal joints can be seen from the trend shown which is linear and tends to increase. The higher the flow rate of the shielding gas, the greater the maximum tensile stress produced in the bimetallic joint.

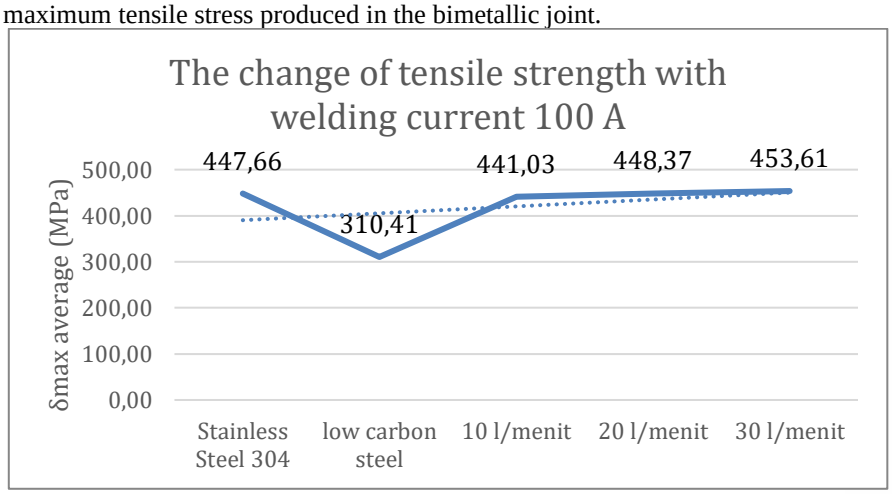

Figure 2. Graph of changes in tensile strength at a current of 100 A

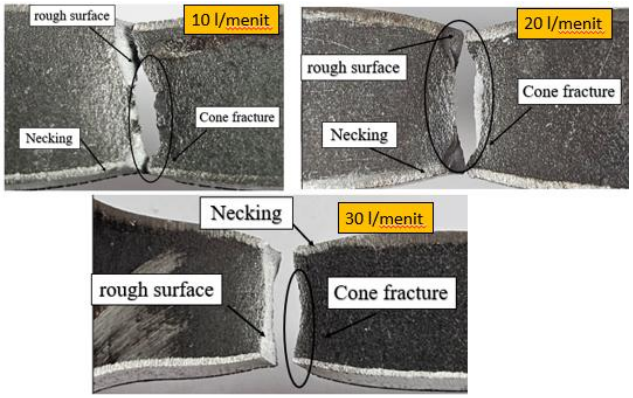

Figure 3. Macrofracture of tensile strength at a current of 100 A

At a gas flow rate of 10 l/minute, the tensile strength is quite high, namely 441.0269 MPa. Then it increased to a variation of 20 l/minute, namely 448.3745 MPa. When the gas flow rate was increased again to 30 l/min, there was still an increase in the tensile strength to 453.6147 MPa. The increase that occurred was not very significant from each variation. At a gas flow rate variation of 10 l/min, the welded joint was well protected, but increasing the gas flow rate to 20 and 30 l/min showed that a larger shielding gas had a better effect on the joint quality. This is because the higher the gas flow rate, the greater the gas's ability to remove oxygen, nitrogen and other elements that can reduce the quality of the welded joint. Better protection results in stronger connections and higher maximum tensile stress. Based on the macro photo of the tensile test results in Figure 3, for all variations in gas flow rate from 10 l/min to 30 l/min, the fracture occurred in the basemetal area and the fracture was ductile. This happens because it is characterized by necking, which is an indication of plastic deformation before fracture.

b. Effect of varying gas flow rate on welding current 120A

Based on the graph in Figure 4, the tensile strength of the bimetallic connection of low carbon steel plate and stainless steel 304 at a current of 120 A has a different trend. At a gas flow rate of 10 l/min, the tensile strength is relatively low, namely 297.9797 MPa. Then there was a significant increase in the variation of 20 l/minute, namely 431.8566 MPa. This value is the highest tensile strength of the other variations. However, when the gas flow rate was increased again to 30 l/min, the tensile strength decreased to 318.4333 MPa. Based on the macro photo of the tensile test fracture results in Figure 5, it shows that at gas flow rates of 10 and 30 L/minute, the fracture is brittle and occurs in the HAZ area. When compared with the decrease in tensile strength that occurs in this variation, this is possible because there is an inappropriate gas flow at the 120A current, resulting in rapid cooling and creating a more brittle structure. A gas flow rate of 20 L/min is the optimal condition for this flow. The highest tensile strength occurs at a gas flow rate of 20 l/minute, where the fracture results from the tensile test occur in the basemetal area and the fracture nature is ductile.

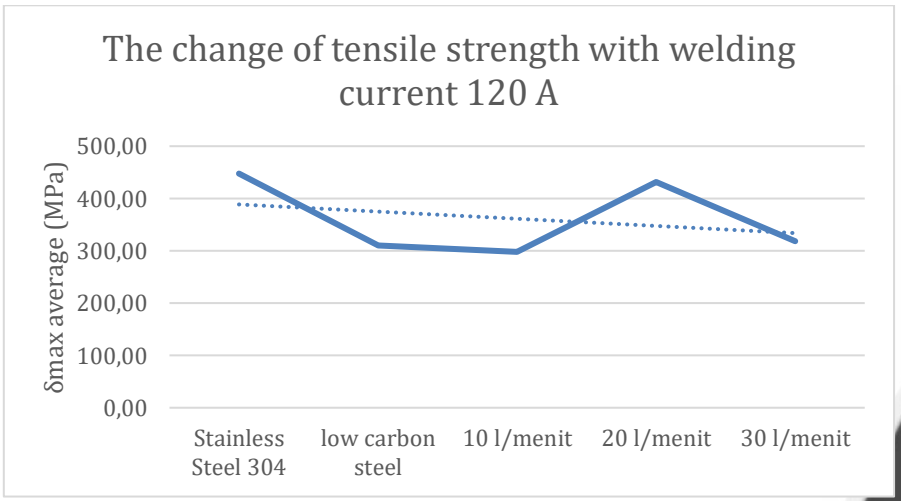

Figure 4. Graph of changes in tensile strength at a current of 120 A

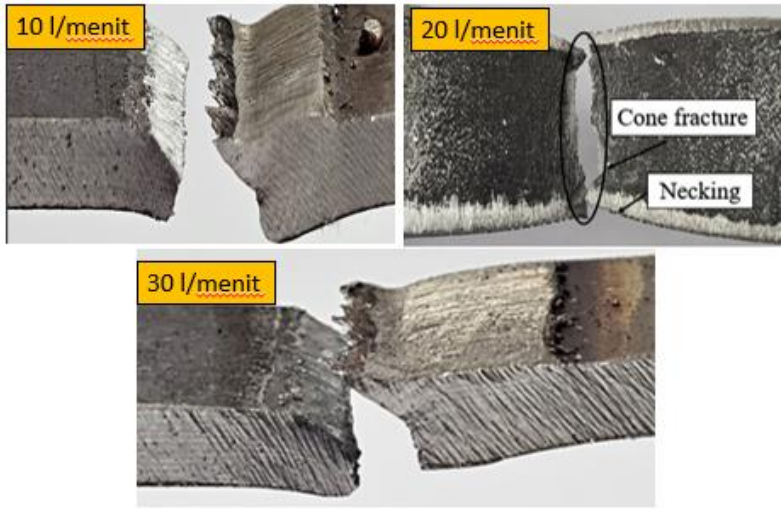

Figure 5. Macrofracture of tensile strength at a current of 120 A

c. Effect of varying gas flow rate on welding current 140A

Based on the graph in Figure 6, which is a graph of changes in tensile strength at a welding current of 140 A. In the picture, it can be seen that there is a trend of increasing maximum tensile stress along with increasing gas flow rate. This graph pattern is similar to the 100A current graph pattern, where increasing the gas flow rate increases the maximum tensile stress. At a gas flow rate of 10 l/minute, the tensile strength is quite high, namely 441.0058 MPa. Then it increased to a variation of 20 l/minute, namely 455.3382 MPa. When the gas flow rate was increased again to 30 l/min, there was still an increase in the tensile strength to 466.3382 MPa. Increasing the gas flow rate from 10 L/min to 30 L/min resulted in an increase in the maximum tensile stress of approximately 25.33 MPa.

In this current, the fracture form from the tensile test results is shown in Figure 7. Fractures at varying gas flow rates of 10 l/minute and 30 l/minute occurred in the basemetal with ductile fracture character. At a gas flow rate of 20 l/min, fracture occurred in the basemetal which was close to the HAZ, but the fracture character was still ductile, because there was a reduction in the dimensions of the fracture. Even though the gas flow rate was increased by welding at a current of 140 A, the welding results are more stable and produce a strong joint.

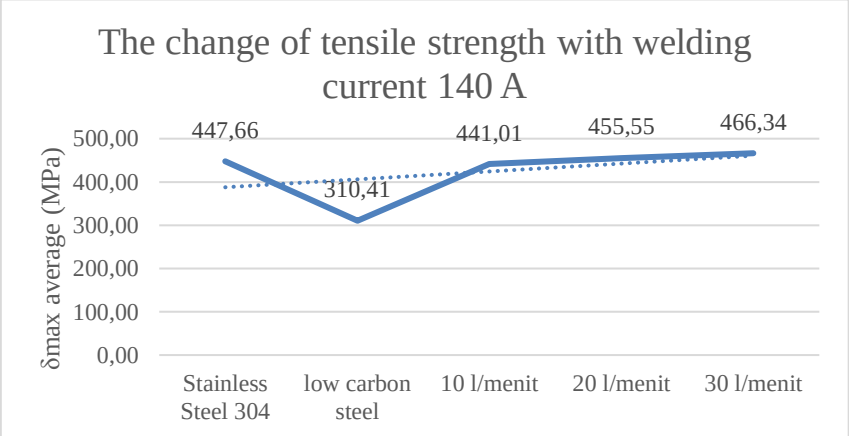

Figure 6. Graph of changes in tensile strength at a current of 140 A

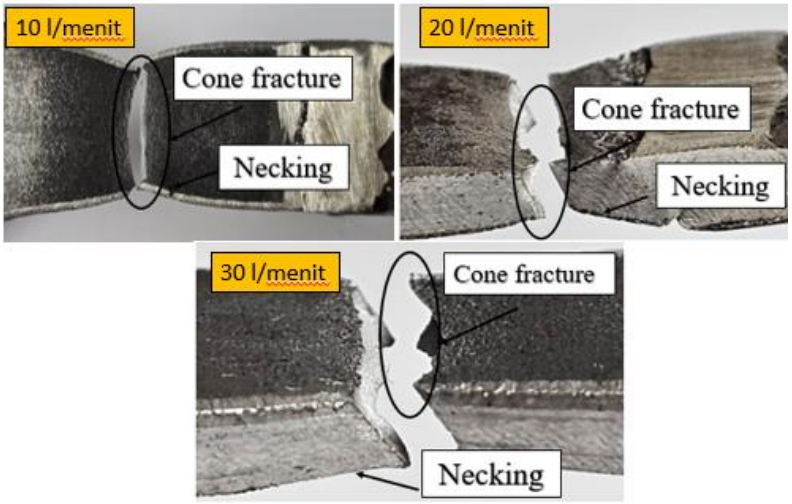

Figure 7. Macrofracture of tensile strength at a current of 140 A

d. Effect of varying gas flow rate on welding current 160A

Based on data on variations in gas flow rate towards the maximum tensile stress of the bimetal joint in Figure 8, the graphic trend shown tends to form a non-linear trend where at a gas flow rate of 10 L/minute, the maximum tensile stress is at a high point, namely 448.4457 MPa. When the gas flow rate was increased to 20 L/minute, the tensile stress actually decreased to 420.5255 MPa. Then, when the gas flow rate was increased to 30 l/min, the tensile stress increased again with a result of 448.4173 MPa, this tensile stress was almost the same as the variation of 10 l/min. Under these conditions, the optimal gas flow rate is around 10 L/min and 30 L/min, while 20 L/min may not provide ideal conditions for the formation of a strong joint. Based on the fracture shape of the tensile test results shown in Figure 9, at a flow of 160 L/min it was found that there was a significant difference between gas flow rates of 10 l/minute and 30 l/minute, both of which produced fractures in the HAZ with a brittle character. However, at a gas flow rate of 20 l/min, fracture occurred in the base metal with ductile character. This indicates that at higher flows, control of the gas flow rate becomes more critical, as too high or too low a rate can result in brittle fracture and lower tensile strength.

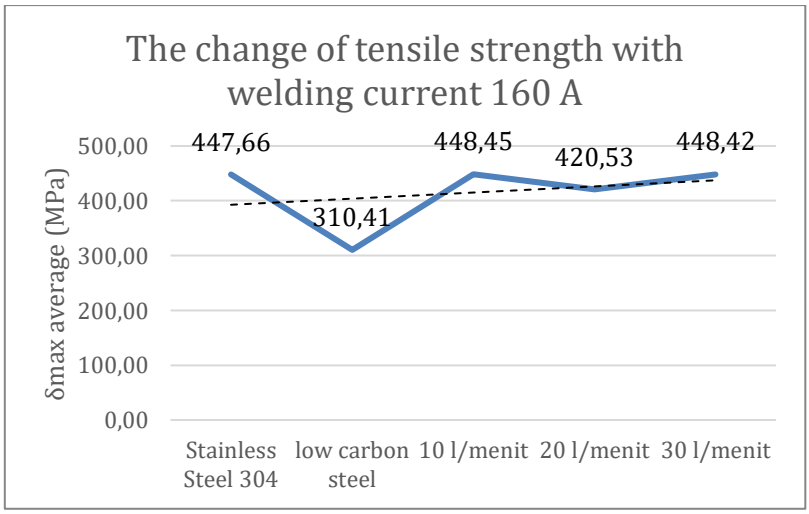

Figure 8. Graph of changes in tensile strength at a current of 160 A

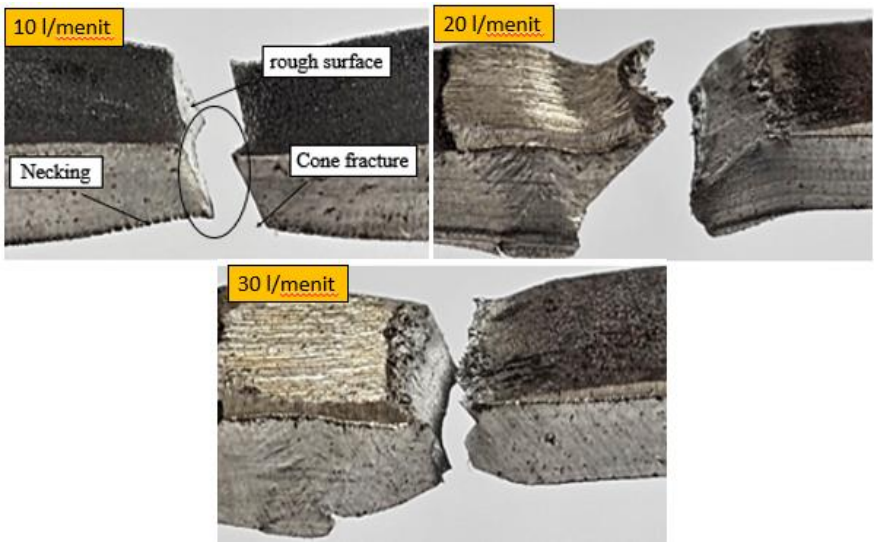

Figure 9. Macrofracture of tensile strength at a current of 160 A

e. Effect of varying gas flow rate on welding current 180A

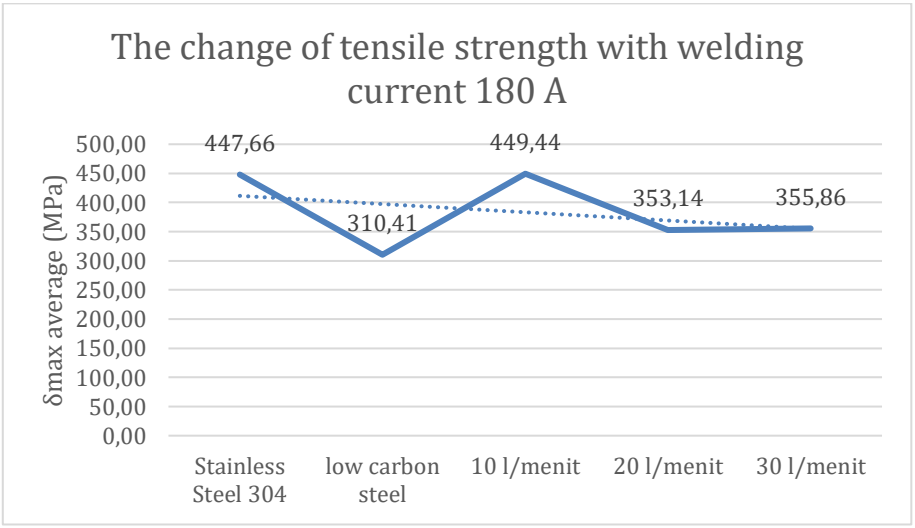

Figure 10. Graph of changes in tensile strength at a current of 180 A

Based on data on variations in gas flow rate towards the maximum tensile stress of the bimetal joint in Figure 10, the graphic trend shown tends to decrease. At a rate of 10 l/min, the maximum tensile stress is 449.4356 MPa with fracture occurring in the basemetal and its ductile nature, and there is necking. At a rate of 20 l/min, the tensile stress dropped drastically to 353.1441 MPa, with ductile fracture occurring in the base metal. The fracture form is shown in Figure 11. At a rate of 30 l/min, the tensile stress slightly increases to 355.8598 MPa with ductile fracture and remains in the base metal. This shows that at very high currents, despite ductile deformation, the maximum tensile strength decreases. This decrease in tensile strength is likely due to overheating which can cause degradation of the mechanical properties of the material.

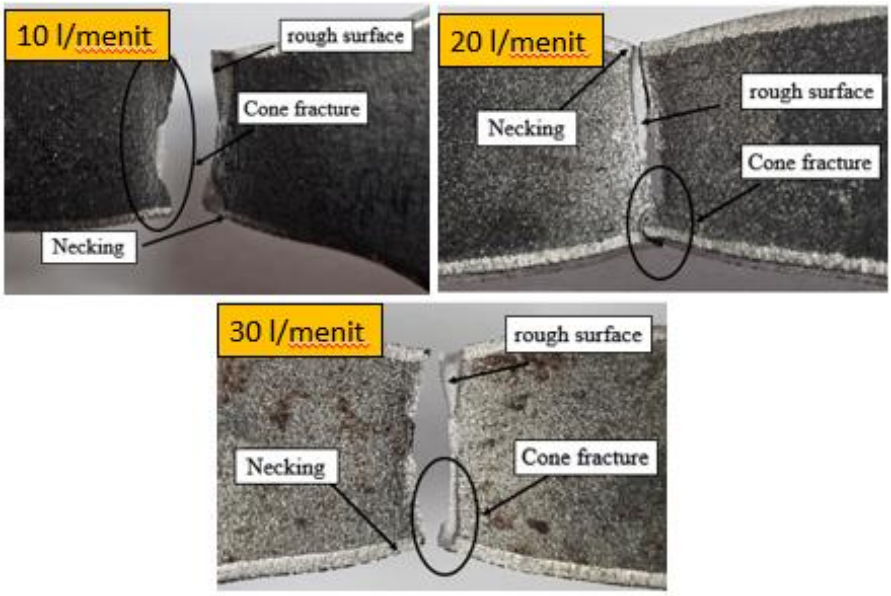

Figure 11. Macrofracture of tensile strength at a current of 180 A

3.2. Discussion

Based on the all graphs of the effect of gas flow rate on the tensile strength of the weld, and and the fracture shape, it can be concluded that variations in gas flow rate parameters in the welding process have a significant influence on the tensile strength and shape of the fracture in the weld. The gas flow rate functions to protect the molten metal from oxidation and contamination from external air (such as oxygen and nitrogen). In this research, varying gas flow rates influence the results of the tensile strength of the welded joint and its fracture characteristics, both in terms of the location of the fracture and the type of fracture that occurs.

If the gas flow rate is too low, the shielding gas may not be sufficient to protect the weld area from air contamination. This can cause oxidation or other contamination that results in weld defects, such as porosity and slag inclusion [9] [19]. As a result, the tensile strength of the weld will decrease due to the presence of weak points in the weld joint structure. For example, at a gas flow rate of 10 l/min with a current of 120A and 160A, a fracture occurred in the HAZ with brittle fracture characteristics, indicating that the low gas flow rate was not sufficient to protect the weld from atmospheric influences.

If the gas flow rate is at an optimal level, namely at a current of 100A and a gas flow rate of 20 l/minute, the protective gas will be effective in protecting the welding area from contamination. This allows the formation of a cleaner weld joint, free from weld defects, thereby increasing the tensile strength of the weld. Apart from that, the gas flow rate is too high, namely at a current of 180A with a gas flow rate of 30 l/minute, the tensile strength decreases to 355.8598 MPa. High gas flow rates can cause turbulence effects in the welding area, which actually causes atmospheric air to be drawn into the welding area. In addition, too heavy a gas flow can disrupt the stability of the welding arc, resulting in poor weld quality.

Effect of gas flow in the welding process According to Swami (2018), the flow of protective gas such as argon or CO2 functions to protect the welding area from air contamination, which can reduce the quality of the joint [17]. In this study, the effect of gas flow rate is clearly visible, especially at currents of 100A to 140A, where increasing the gas flow rate causes a significant increase in the maximum tensile strength. For example, at a current of 140A, the tensile strength increases from 441.0058 MPa (10 L/min) to 466.3382 MPa (30 L/min). This indicates that sufficient shielding gas helps prevent porosity and other defects

4. CONCLUSION

Overall, variations in the optimal gas flow rate produce different maximum tensile strengths, depending on the welding current. Optimal conditions are generally found at a moderate gas flow rate of 20 l/minute. At this gas flow rate the tensile strength is 353.1442 MPa– 455.5458 MPa. The fractures that occur are almost all in the base metal and are ductile in nature, even though at a current of 160 A the fractures occur in the HAZ area, but the tensile strength is still high. A gas flow rate that is too low or too high can cause defects in the joint and reduce the tensile strength of the weld.

5. REFERENCES

[1] M. Choirul U. Nuha and Samsudi, "Pengaruh variasi kuat arus dan tekanan gas pelindung terhadap kekuatan tarik hasil pengelasan MIG (metal inert gas) pembuatan front chasis mobil listrik dengan bahan ST 60," *J. Mech. Eng. Learn.*, vol. 11, no. 2, pp. 1–11, 2022.

[2] T. Abe and H. Sasahara, "Dissimilar metal deposition with a stainless steel and nickel-based alloy using wire and arc-based additive manufacturing," *Precis. Eng.*, vol. 45, pp. 387–395, 2016, doi: https://doi.org/10.1016/j.precisioneng.2016.03.016.

[3] R. Mittal and B. S. Sidhu, "Metallurgical aspects of dissimilar metal weldments : A Review," *Int. Conf. Adv. Futur. Trends Mech. Mater. Eng.*, no. June, pp. 1–8, 2015.

[4] J. P. Oliveira *et al.*, "Dissimilar laser welding of a CoCrFeMnNi high entropy alloy to 316 stainless steel," *Scr. Mater.*, vol. 206, p. 114219, 2022, doi: https://doi.org/10.1016/j.scriptamat.2021.114219.

[5] A. B T, J. Devasia, T. Krishna, and M. T. Kuruvila, "Manufacturing of a bimetallic structure of stainless steel and mild steel through wire arc additive manufacturing – A Critical Review," *Int. J. Innov. Sci. Res. Technol.*, vol. 5, no. 6, pp. 679–685, 2020, doi: 10.38124/ijisrt20jun583.

[6] T. Lei, Y. Rong, H. Wang, Y. Huang, and M. Li, "A review of vision-aided robotic welding," *Comput. Ind.*, vol. 123, p. 103326, 2020, doi: https://doi.org/10.1016/j.compind.2020.103326.

[7] B. B. Sherpa and R. Rani, "Explosive welding process to clad materials with dissimilar metallurgical properties," S. Kumar, Ed. Rijeka: IntechOpen, 2021, p. Ch. 2. doi: 10.5772/intechopen.94448.

[8] B. Mvola and P. Kah, "Effects of shielding gas control: welded joint properties in GMAW process optimization," *Int. J. Adv. Manuf. Technol.*, vol. 88, no. 9, pp. 2369–2387, 2017, doi: 10.1007/s00170-016-8936-2.

[9] R. Bintarto, M. S. Ma'arif, D. Widhiyanuriyawan, T. D. Widodo, R. Raharjo, and N. A. Purnomo, "Pengaruh laju alir tungsten in-ert gas terhadap kekuatan tarik dan kejut pada sambungan las tig baja galvanis dan aluminium 5052 dengan filler Al-Si 4043," *J. Rekayasa Mesin*, vol. 14, no. 1, pp. 1–12, 2023, doi: 10.21776/jrm.v14i1.656.

[10] C. Cai, S. He, H. Chen, and W. Zhang, "The influences of Ar-He shielding gas mixture on welding characteristics of fiber laser-MIG hybrid welding of aluminum alloy," *Opt. Laser Technol.*, vol. 113, pp. 37–45, 2019, doi: https://doi.org/10.1016/j.optlastec.2018.12.011.

[11] X. Yang, H. Chen, Z. Zhu, C. Cai, and C. Zhang, "Effect of shielding gas flow on welding process of laser-arc hybrid welding and MIG welding," *J. Manuf. Process.*, vol. 38, pp. 530–542, 2019, doi: https://doi.org/10.1016/j.jmapro.2019.01.045.

[12] G. Campana, A. Ascari, A. Fortunato, and G. Tani, "Hybrid laser-MIG welding of aluminum alloys: The influence of shielding gases," *Appl. Surf. Sci.*, vol. 255, no. 10, pp. 5588–5590, 2009, doi: https://doi.org/10.1016/j.apsusc.2008.07.169.

[13] Sarjiyana, Subagiyo, and L. Agustriyana, "Kekuatan tarik pada pengelasan bimetal plat baja karbon rendah dan stainless steel 304 dengan las GMAW," *Jurnal Energi dan Teknologi Manufaktur (JETM)*, vol. 4, no. 2, pp. 7–12, 2021.

[14] A. L. Kurniawan and E. Pranatal, "Analisis kekuatan sambungan las pada plat untuk dek kapal berbahan plat baja A36 terhadap sifat fisis dan mekanis dengan metode pengelasan MIG," *J. Sumberd. Bumi Berkelanjutan*, vol. 1, no. 1, pp. 327–331, 2022, doi: 10.31284/j.semitan.2022.3284.

[15] W. Marthiana, Y. Mahyoedin, D. Duskiardi, and A. Rahim, "Analisa pengaruh variasi arus listrik pengelasan terhadap kekuatan sambungan pengelasan MIG pada material ST 37," *J. Kaji. Tek. Mesin*, vol. 5, no. 2, pp. 140–144, 2020, doi: 10.52447/jktm.v5i2.4217.

[16] R. J. Dimu and O. D. Rerung, "Kekerasan material baja karbon rendah pada daerah lasan TIG dan MIG," *J. Tek. mesin*, vol. 2, no. 1, pp. 12–19, 2019.

[17] S. A. Swami, S. Jadhav, and A. Deshpande, "Influence of MIG Welding process parameters on tensile properties of mild steel.," *Eur. J. Eng. Technol. Res.*, vol. 1, no. 2, pp. 1–5, 2018, doi: 10.24018/ejeng.2016.1.2.133.

[18] S. Singh, V. Kumar, S. Kumar, and A. Kumar, "Variant of MIG welding of similar and dissimilar metals: A review," *Mater. Today Proc.*, vol. 56, pp. 3550–3555, 2022, doi: https://doi.org/10.1016/j.matpr.2021.11.287.

[19] C. Zhu, X. Tang, Y. He, F. Lu, and H. Cui, "Effect of preheating on the defects and microstructure in NG-GMA welding of 5083 Al-alloy," *J. Mater. Process. Technol.*, vol. 251, pp. 214–224, 2018, doi: https://doi.org/10.1016/j.jmatprotec.2017.08.037.

[20] K. Witono, T. Machfuroh, S. Sarjiyana, and E. Faizal, "Pengaruh variasi travel speed terhadap kekuatan tarik pada pengelasan disimilar metal dengan MIG robotic welding," *Otopro*, vol. 19, no. 1, pp. 34–39, 2023, doi: 10.26740/otopro.v19n1.p34-39.

LOGIC
Journal of Engineering Design and Technology
Vol. 24 No.3 November 2024 ; p. 150 - 159

p-ISSN : 1412-114X
e-ISSN : 2580-5649
http://ojs2.pnb.ac.id/index.php/LOGIC

ANALYSIS OF THE EFFECT EVAPORATOR FAN ROTATION VARIATIONS ON AIR BLAST FREEZER PERFORMANCE FOR FREEZING MANGO PUREE

Wardika[1)], Yudhy Kurniawan[2)], Aa setiawan[3)], Muchammad Zuhda Alifun Naja[4)]

1,2,3,4) Refrigeration and Air Conditioning Engineering, Indramayu State Polytechnic, Indramayu, Indonesia

Correponding email [1)] :
wardika8@gmail.com

Abstract. Mangoes are the main commodity in Indramayu Regency, but they are easily damaged after harvesting due to improper mango processing. One solution to overcome this problem is to process mangoes into puree. This process requires freezing technology such as an air blast freezer machine. The evaporator fan functions to prevent blocking of the evaporator fins and distribute cold air so that the room temperature reaches -18˚C. This research aims to determine the effect of variations in evaporator fan rotation on the performance of the air blast freezer system. Data are taken every 10 minutes until the mango puree reaches the set point temperature. Three experiments were conducted with evaporator fan speeds set to low (1800 RPM), medium (2200 RPM), and high (2600 RPM). Based on the tests that have been carried out, the system performance at low fan rotation produces an actual Coefficient of Performance (COP) of 1.9 with an efficiency of 41% and electricity costs of IDR 462,900. Medium fan rotation produces an actual COP of 2.0 with an efficiency of 43% and electricity costs of IDR 469,380. High fan rotation produces an actual COP of 2.1 with an efficiency of 45%. This research shows how variations in fan speed affect the COP, system efficiency, and operational costs, therefore the results of this research contribute to the development of energy efficient and economical cooling technology, especially for tropical-based food preservation applications such as fruit puree mango.

Keywords : Mango, Puree, Air Blast Freezer, Fan, Performance.

1. INTRODUCTION

Mango fruit is a fruit that contains various vitamins and minerals. One of the problems faced in developing mango fruit is that it is easily damaged, so its shelf life is relatively short. This causes high post-harvest yield losses during the main harvest and causes the selling price of mangoes to decline. Preserving mango puree is important because mangoes have a short shelf life due to their high water content, and are susceptible to post-harvest damage. The transformation of mango into puree allows the product to last longer and can be used as a raw material for the food industry [1]. So that consumers can still enjoy mangoes outside of the harvest season, there needs to be a process for processing mangoes into puree. The shelf life of mango puree really depends on the storage temperature. From the research that has been carried out, the longest estimated shelf life is for puree pasteurized at a temperature of 65 °C with a storage temperature of 7 °C, namely 11.2 months. The shortest estimated shelf life was obtained for puree stored at a temperature of 30 °C, namely 0.95 – 1.1 month [2].

Processing mango puree will definitely require cooling system technology such as an Air Blast Freezer machine. The fast-freezing method (Air Blast Freezer) was chosen because the fast cooling process can help prevent the growth of microorganisms during post-harvest mango processing more effectively than the regular freezing method. This system uses a fan to distribute cold air efficiently, ensuring a homogeneous temperature across the product surface. In addition, fast freezing with an air blast freezer preserves the texture, color and nutrition of mango puree better than the slow freezing method, which can cause cell damage. Other methods, such as static

freezing or using liquid nitrogen, do not provide adequate air circulation, which can lead to the formation of large ice crystals, damaging the product structure [3].

The function of the fan is to distribute the cold air produced by the evaporator throughout the room. The use of fans is intended to ensure that the room and product temperatures reach the target temperature, namely -18 ˚C. The rate of air flow entering the evaporator greatly influences the system performance (coefficient of performance) in the refrigeration system [4]. The problem above is to determine the performance of an air blast freezer system when using three variations of evaporator fan, namely low, medium and high.

2. METHODS

The stages of conducting the research were carried out based on the flowchart shown in Figure 1. At the data collection stage, the author will take data from the refrigeration system at the point of condenser in and out temperature (˚C), evaporator in and out temperature (˚C), suction and exhaust pressure (psi), product temperature (˚C), and cabin temperature (˚C). Meanwhile, environmental conditions during testing were adjusted to the average temperature of Indramayu Regency during the day, namely 33 °C. Then data are collected every 10 minutes until the mango puree reaches a temperature of -18 °C. The data analysis stage was obtained from the results of data collection by calculating engine performance and comparing engine performance between air blast freezer systems using variations in low, medium and high evaporator fan rotation. The fan speed variations were selected based on significant differences in Air Blast Freezer (ABF) system performance. 1800 RPM (low) is a representation of energy saving conditions with slow air distribution. 2200 RPM (medium) represents a balanced speed that aims to optimize energy efficiency and cooling performance. 2600 RPM (high), which is the maximum speed for fast air distribution and even freezing in a short time. The selection of the RPM value is based on the voltage output setting via the dimmer and adjusted to the evaporator fan capacity.

2.1 Research Design

A process or stage of working on a final project that starts from start to finish. The following is a diagram of the stages of work in the final project research.

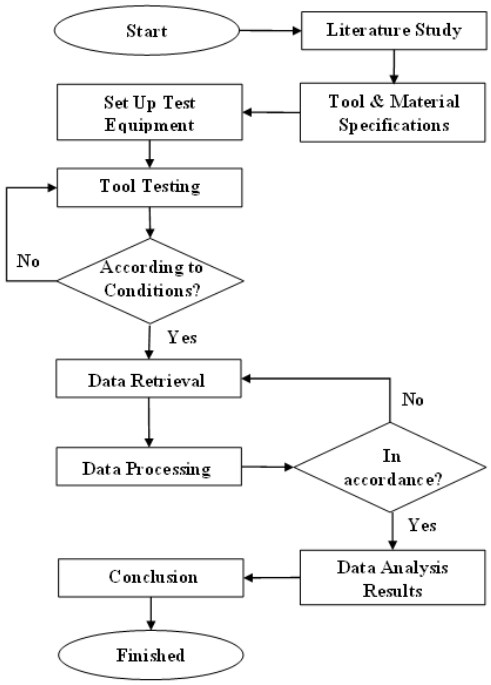

Figure 1. Research Flow Chart

2.2 Set Up Test Equipment

The test equipment used in this research includes a 2 PK refrigeration compressor and an upright chiller evaporator, which is equipped with an evaporator fan. The evaporator has been modified for low temperature operation by adding several components, including a hot gas pipe from the discharge line. This pipe channels hot steam to melt the ice and prevent blockages in the evaporator coil, with manual control via a push button. The hot gas will work for 2 minutes after the cooling time lasts for 60 minutes. Three fans in front of the evaporator which function to increase the air flow rate in the evaporator. The cooling room uses an iron plate and sandwich panel structure with a thickness of 5 cm and dimensions of 1 x 1.5 x 1 m. Table 1 shows the component specifications used in this

research.

Table 1. Component Specifications

No	Component	Quantity	Unit	Information
1	Compressor	1	Unit	Hermetic 2 PK
2	Condensor	1	Unit	Air cooled
3	Capillary tube	200	cm	Diameter 0,7
4	Evaporator	1	Unit	Air cooled
5	Fan Evaporator	3	Unit	Axial fan
6	Ampere pliers	1	Unit	Model 2007R
7	Thermometer	5	Unit	Elitech
8	Digital Thermostat	1	Unit	Model Elitech STC 8080HX
9	Pressure gauge	2	Unit	Model HC-OG-3.8
10	Manifold gauge	1	Unit	R-404A
11	Vacum pump	1	Unit	Power 1/8 HP
12	Dimmer	1	Unit	Model SCR2000W
13	Tachometer	1	Unit	Model DT2234
14	Refrigerant	1	Can	R-404A Chemours

2.3 Tool testing

The composition of the air blast freezer system components for freezing mango puree is arranged according to figure 2. A compressor (1) will work on the refrigerant by pumping refrigerant throughout the system, so that the refrigerant has high pressure and temperature, the high pressure refrigerant will flow to the condenser (2) because the condenser temperature is higher than the ambient temperature, the refrigerant heat will be released through the condenser pipe walls into the surrounding environment. A filter dryer (3) is used to filter dirt in a system so that the dirt does not circulate with the refrigerant which could potentially cause congestion in the system. Capillary pipe (5) is used to reduce the pressure in a system so that the refrigerant temperature is lower than the temperature of the room to be cooled. Evaporator (6) is used as a heat absorber in the cabin. A cabin has the function of storing research materials carried out. An evaporator fan is used as an aid in distributing cold air produced by the evaporator (6) into the cabin.

An accumulator (7) is used to hold liquid refrigerant to ensure that the refrigerant entering the compressor (1) has a gas phase. The hot gas defrosts solenoid valve (8) functions if a vapor compression system wants to utilize hot vapor refrigerant from the compressor (1) to help melt the frost contained in the evaporator (6).

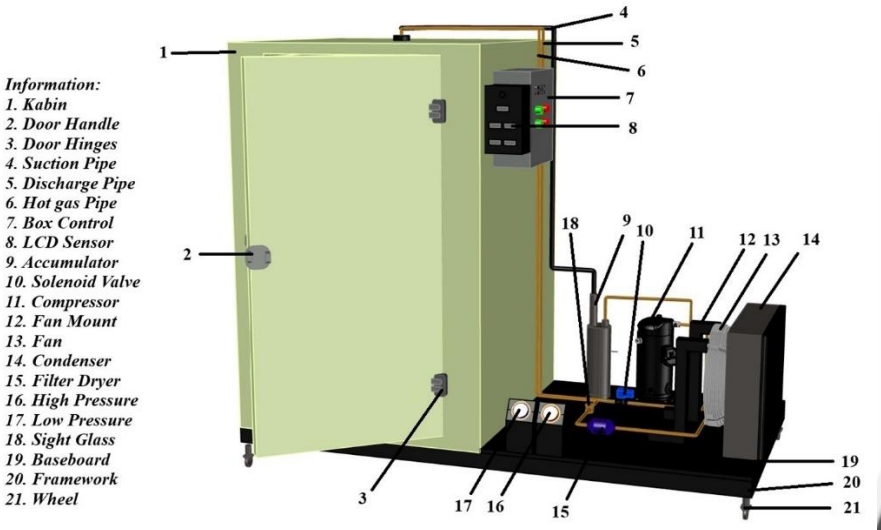

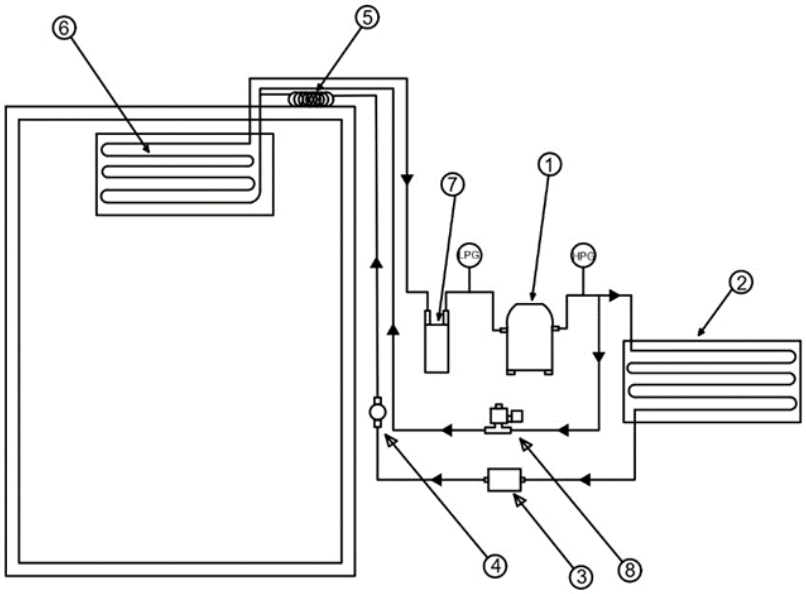

Figure 2. Air Blast Freezer Installation Scheme

Information:

1. Compressor
2. Condensor
3. Filter Dryer
4. Sight Glass
5. Capillary tube
6. Evaporator
7. Accumulator
8. Solenoid Valve

Testing is carried out by conducting experiments to obtain the desired system conditions. To get the desired temperature, several experiments were carried out. The experiment begins with a running test in an uncontrolled engine condition and by filling the refrigerant based on the pressure and current listed on the nameplate. From the experiments carried out, the temperature values at the inlet and outlet of the evaporator gradually became the same, as a result of this a blockage occurred in the evaporator component. Then the refrigerant is reduced with reference to the R404A refrigerant table, the refrigerant is filled with a pressure of 30 psi on the low pressure side. To overcome the blockage on the evaporator, hot gas defrost is carried out. This defrost time is based on the blocking condition of the evaporator component or is set manually by pressing the push button. When the push button is pressed, solenoid valve 1 (defrost) works. When and how long the defrost works, experiments are carried out by visually observing the condition of the evaporator. From these observations, it was found that the cooling time was 60 minutes, then defrosting for approximately 2 minutes. Determining the cooling time and defrost time incorrectly will affect the system, such as the compressor shutting down because the pressure is too low or the compressor shutting down because it overheats.

2.4 Data Retrieval

The steps taken after testing the system include collecting data, which will later be analyzed. This was done to determine the comparison of the air blast freezer machine with variations in rotation of the evaporator fan. The data that will be taken is the temperature of the mango puree. Before data collection, due to the unavailability of mango puree products in the required amount, 5 kg of mango puree was used. To meet the load requirement of 50 kg, bottled water in packaging was added as a substitute for mango puree.

In initial conditions, the product has a temperature of 27 – 30 °C. Data collection was carried out until the mango puree temperature reached -18 °C. The data collection process was carried out in 3 different experiments. The first data collection was carried out by varying the evaporator fan rotation low, with an rpm value set at 1800. The second data collection was carried out by varying the medium evaporator fan rotation, with an rpm value set at 2200. The third data collection was carried out by varying the evaporator fan rotation high, with the rpm value is set at 2600 rpm. The existing data was obtained from careful and direct observations. Required data includes discharge pressure, suction pressure, temperatures for the evaporator (in and out), condenser (in and out), cabin temperature, voltage, and current.

3. RESULTS AND DISCUSSION

Based on the results of data collection, data processing was carried out using the P-H diagram of R-32 refrigerant. Based on the results of the P-H diagram plot, the enthalphi value for each measurement variable is obtained and

then the calculation is carried out using the following equation:

Compression work

$$qw = h2 - h1 \quad (1)$$

$$Qe = m \times qw \quad (2)$$

Heat release in the condenser

$$qc = h2 - h3 \quad (3)$$

$$Qc = m \times qc \quad (4)$$

Evaporation process

$$qe = h1 - h4 \quad (5)$$

$$Qe = m \times qce \quad (6)$$

COP calculation

$$COPcarnot = \frac{T\ evaporasi}{T\ kondensasi - T\ evaporasi} \quad (7)$$

$$COPaktual = \frac{h1-h4}{h2-h1} \quad (8)$$

Efficiency Calculations

$$\eta = \frac{COPaktual}{COPcarnot} \times 100\% \quad (9)$$

From the calculation process using the equation above, tables and graphs are obtained regarding the influence of fan speed variations on the performance parameters of the air blast freezer. Table 2 shows the calculation results for various fan variations at 300 minutes.

Table 2. Fan Variation Calculation Results

Variasi Fan	qw (kJ/kg)	qc (kJ/kg)	qe (kJ/kg)	COP aktual	COP carnot	Efisiensi (%)	Temp. Kabin (˚C)
Low	53	155	102	1,9	5	38	-2
Medium	52	154	102	1,9	5	39	-4
High	50	153	103	2	4,5	45	-6

3.1 Effect of Fan Variations on Compression Performance

Based on the graph in Figure 3, it explains that compression work using the 300th minute low evaporator fan research method has a qw value of 53 kJ/kg, while compression work using the 300th minute medium evaporator fan research method has a qw value of 52 kJ/kg , as well as for compression work using the 300th minute high evaporator fan research method, it has a qw value of 50 kJ/kg. This shows that the low evaporator fan research method has the largest qw or compression work value compared to the medium evaporator fan and high evaporator fan research methods. This is because the low evaporator fan research method has a large evaporation work value compared to the medium evaporator fan and high evaporator fan research methods. In this air blast freezer system there is a defrost system, which occurs when the system works once every 60 minutes which causes a temporary increase in temperature in the evaporator, thus affecting the graph of the compression process.

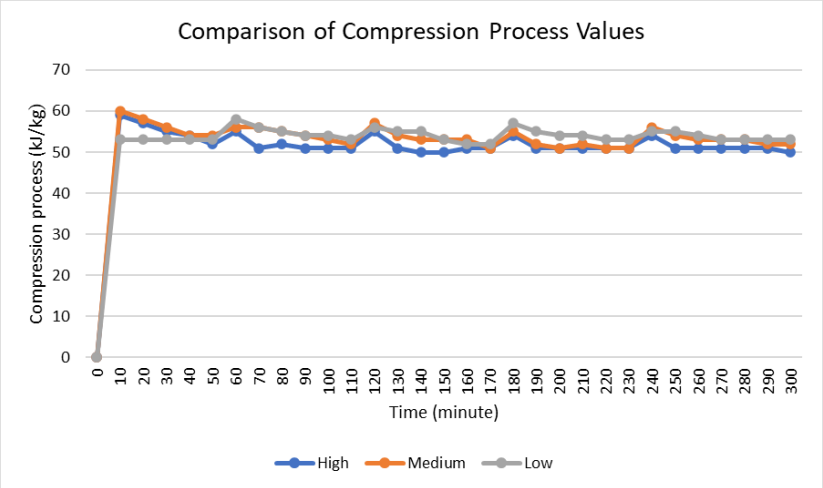

Figure 3. Comparison of Compression Work Values (qw) on Fan Variations

3.2. Effect of Fan Variations on Condensation Performance

Based on the graph in Figure 4, it explains that condenser work using the 300th minute low evaporator fan research method has a qc value of 155 kJ/kg, while condenser work using the 300th minute medium evaporator fan research method has a qc value of 154 kJ/kg , as well as for condenser work using the 300th minute high evaporator fan research method, it has a qc value of 153 kJ/kg. This shows that the low evaporator fan research method has the greatest qc or condenser work value compared to the medium evaporator fan and high evaporator fan research methods. This is because the heat capacity removed is smaller compared to the medium evaporator fan and high evaporator fan research methods. In this air blast freezer system there is a defrost system, which occurs when the system works once every 60 minutes which causes a temporary increase in temperature in the evaporator, thus affecting the graph of the condensation process.

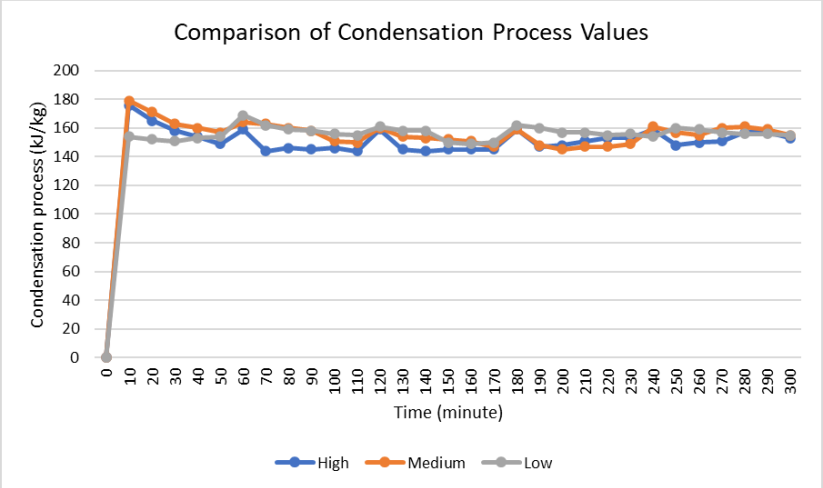

Figure 4. Comparison of Condensation Work Values (qc) on Fan Variations

3.3 Effect of Fan Variations on Evaporation Performance

Based on the graph in Figure 5, it explains that the evaporator work using the low evaporator fan research method at the 300th minute has a qe value of 102 kJ/kg, while the evaporator work using the medium evaporator fan research method at the 300th minute has a qe value of 102 kJ/kg. , as well as for evaporator work using the 300th minute high evaporator fan research method, the qe value is 103 kJ/kg. This shows that the low evaporator fan research method has the largest qe or evaporator work value compared to the medium evaporator fan and high evaporator fan research methods. This is because using a low fan has the effect of holding the air in contact with the evaporator longer so that more heat is absorbed compared to medium and high. In this air blast freezer system there is a defrost system, which occurs when the system works once every 60 minutes which causes a temporary increase in temperature in the evaporator, thus affecting the graph of the evaporation process.

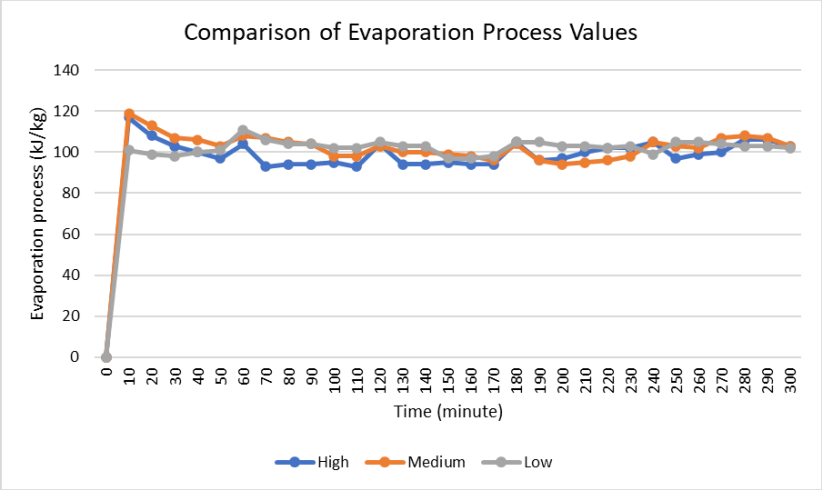

Figure 5. Comparison of Evaporation Work Values (qe) in Fan Variations

3.4 Effect of Fan Variations on Cabin Temperature

Based on the graph in Figure 6, it explains that the cabin temperature using the 300th minute low evaporator fan research method reached a temperature of –2˚C, while the cabin temperature using the 300th minute medium evaporator fan research method reached a temperature of -4˚C, as well as for the The cabin using the 300th minute high evaporator fan research method reaches a temperature of -6˚C. This shows that by using variations in high evaporator fan rotation, the cabin temperature decreases more quickly compared to variations in low evaporator fan rotation and medium evaporator fan rotation. This is because by varying the high evaporator fan rotation, the cold air distribution process is more evenly distributed more quickly. In this air blast freezer system there is a defrost system, which occurs when the system works once every 60 minutes which causes a temporary increase in temperature in the evaporator, thus affecting the cabin temperature graph.

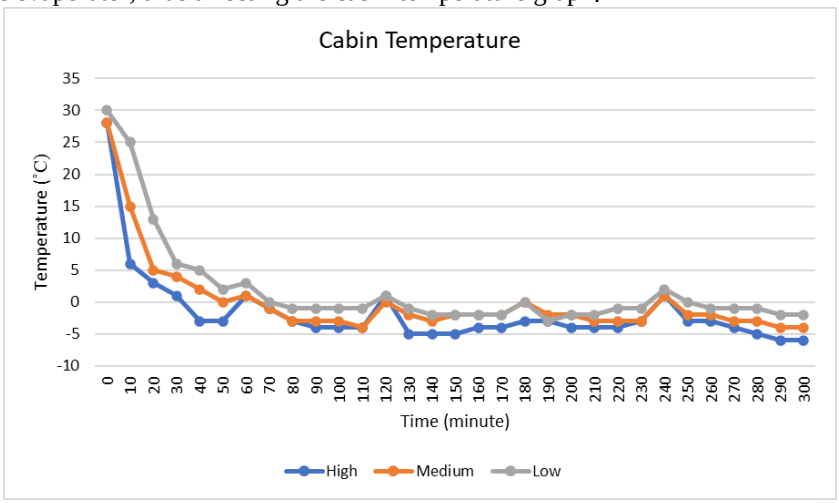

Figure 6. Cabin Temperature Comparison

3.5 Effect of Fan Variations on Actual COP Values

Based on the graph in Figure 7, it explains that the COPActual value using the 300th minute low evaporator fan research method has a COPActual value of 1.9. Meanwhile, the COPActual value using the 300th minute medium evaporator fan research method has a COPActual value of 1.9 and the COPActual value using the 300th minute high evaporator fan research method has a COPActual value of 2. This shows that with the evaporator fan research method high has the highest COPActual value compared to the low evaporator fan and medium evaporator fan research methods. This is because the high evaporator fan research method has a lower compression work value compared to the low evaporator fan and medium evaporator fan research methods.

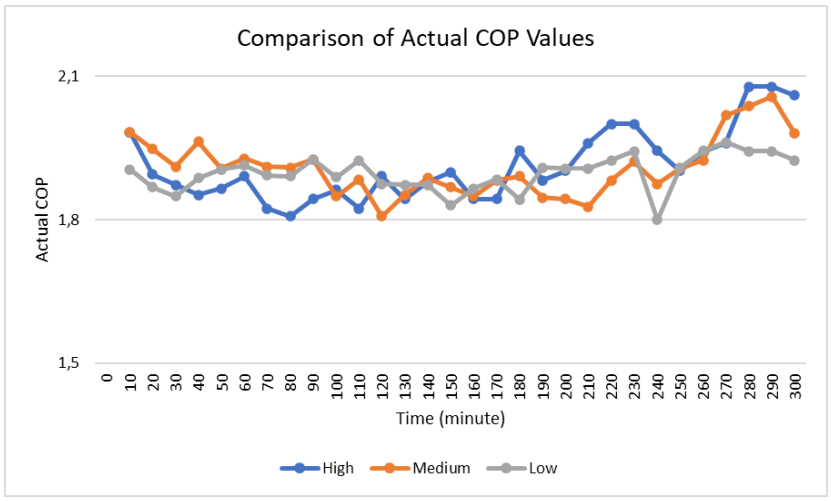

Figure 7. Comparison of Actual COP Values

3.6 Effect of Fan Variations on COP Carnot Values

Based on the graph in Figure 8, it explains that the COPCarnot value using the 300th minute low evaporator fan research method has a COPCarnot value of 5, while the COPCarnot value using the 300th minute medium evaporator fan research method has a COPCarnot value of 5, and for the COPCarnot value with The 300th minute high evaporator fan research method has a COPCarnot value of 4.5. This shows that the low evaporator fan and medium evaporator fan research methods have a higher COPCarnot value compared to the high evaporator fan research method. This is because the temperature in the evaporator is lower compared to the fan evaporator high research method. In this air blast freezer system there is a defrost system, which occurs when the system works once every 60 minutes which causes a temporary increase in temperature in the evaporator, thus affecting the graph on COPCarnot.

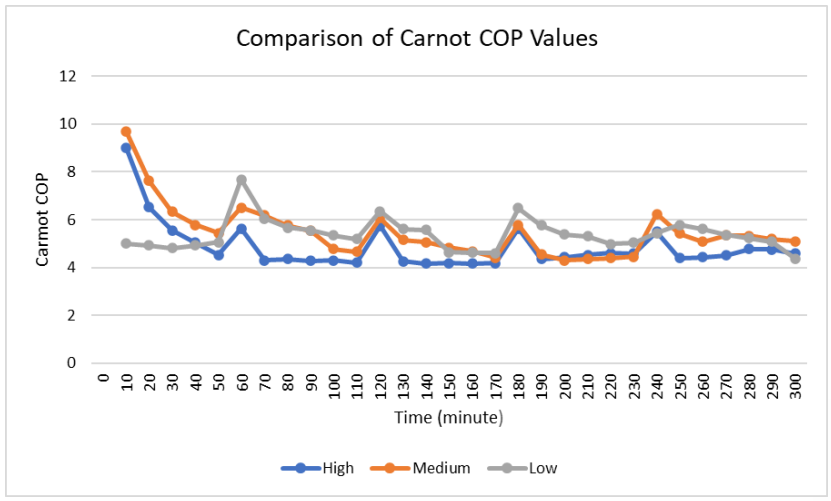

Figure 8. Comparison of Carnot COP Values

3.7 Effect of Fan Variations on Efficiency Values

Based on the graph in Figure 9, it explains that the efficiency value with the 300 minute low evaporator fan research method has an efficiency value of 38%, while the 300 minute medium evaporator fan research method has an efficiency value of 39%, as well as the high minute evaporator fan research method. The 300th has an efficiency value of 45%. This shows that the high evaporator fan research method has the highest efficiency value compared to the low evaporator fan and high evaporator fan research methods. This is because the high evaporator fan research method has a smaller Carnot COP value and the actual COP value is greater compared to the low evaporator fan and medium evaporator fan research methods.

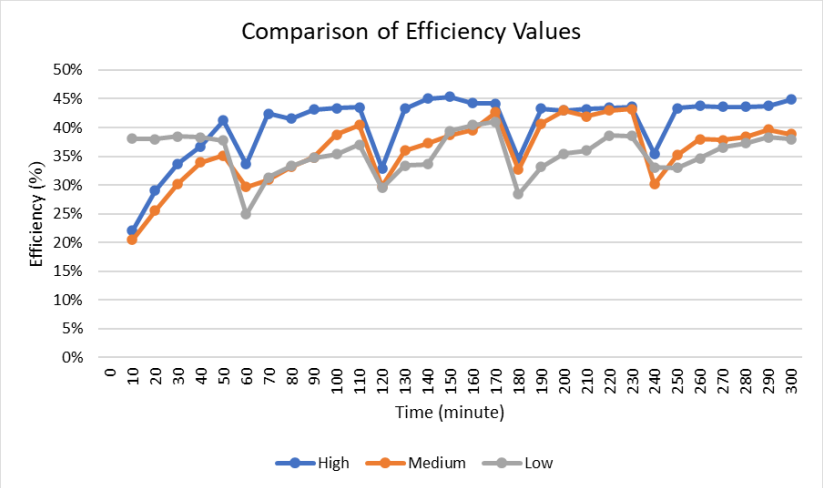

Figure 9. Comparison of Efficiency Values

4. CLOSING

4.1 Conclusion

Based on the results of the research carried out, it can be concluded that in the air blast freezer system, if the evaporator fan rotation is varied, it shows that.

1. For low evaporator fan rotation (1800 RPM), it shows that COPActual has the highest value of 1.9 and the lowest value of 1.8. Besides that, the highest COPCarnot value was 8.6 and the lowest value was 4.6. The highest efficiency achieved was around 41%, while the lowest efficiency reached a value of 22%. In the air blast freezer system, the average COPActual value was 1.9 and the average COPCarnot was 5.8 and the average efficiency value was around 34%.
2. For medium evaporator fan rotation (2200 RPM), it shows that COPActual has the highest value of 2.0 and the lowest value of 1.8. Besides that, the highest COPCarnot value was 9.6 and the lowest value was 4.2. The highest efficiency achieved was around 43%, while the lowest efficiency reached a value of 20%. In the air blast freezer system, the average COPActual value was 1.9 and the average COPCarnot was 5.4 and the average efficiency value was around 36%.
3. For high evaporator fan rotation (2600 RPM), it shows that COPActual has the highest value of 2.1 and the lowest value of 1.8. Besides that, the highest COPCarnot value was 8.9 and the lowest value was 4.1. The highest efficiency achieved was around 45%, while the lowest efficiency reached a value of 22%. In the air blast freezer system, the average COPActual value was 1.9 and the average COPCarnot was 5.1 and the average efficiency value was around 40%.
4. Based on the analysis that has been carried out, all variations of the evaporator fan rotation are not suitable for application in the air blast freezer system, because they do not meet the requirements for achieving a mango puree freezing temperature of -18 °C so they are not able to provide a solution to the problem of post-harvest mango fruit.

5. Acknowledgement

We would like to thank Politeknik Negeri Indramayu under grant PUKTI SIPASTI. The authors fully acknowledged Politeknik Negeri Indramayu for the approved fund, making this research can effective and can implementation.

6. REFERENCES

[1] Aa Setiawan and M. I. Wardika, "Analisis pengaruh variasi putaran extra fan evaporator terhadap kinerja cold storage menggunakan mesin outdoor AC split untuk penyimpanan puree mangga," Jurnal Rekayasa Energi (JRE), vol. 2, no. N, 2023.

[2] A. Wahyudi, "Hot gas defrost," [Online]. Available: https://www.tptumetro.com/2020/07/hot-gas-defrost.html#:~:. [Accessed: Jun. 22, 2023].

[3] M. Almaududi, "Pengaruh laju aliran udara masuk evaporator terhadap kapasitas pendinginan (coefficient of performance) dan kelembapan udara pada sistem refrigerasi air condition," Edu Elektrika Journal, vol. 9, no. 1, pp. 20–23, 2020.

[4] D. Amiarsi and I. Mulyawanti, "Pengaruh metode pembekuan terhadap karakteristik irisan buah mangga beku selama penyimpanan (Effect of freezing method on characteristic of fruit slice of mango during storage)," J. Hortikultura, vol. 23, no. 3, pp. 255–262, 2013.

[5] ASHRAE, ASHRAE Fundamental Handbook. Atlanta: ASHRAE, 2001.
[6] ASHRAE, ASHRAE Refrigeration. Atlanta: ASHRAE, 2010.
[7] ASHRAE, ASHRAE Handbook Refrigeration. Atlanta: ASHRAE, 2018.
[8] E. T. Berman, Teknik Pendingin. 2013.
[9] R. M. Fajarani, Y. Handoyo, and R. H. Rahmanto, "Analisis beban pendinginan pada cold storage untuk penyimpanan daging," Jurnal Ilmiah Teknik Mesin, vol. 7, no. 1, pp. 12–22, 2019. DOI: 10.33558/jitm.v7i1.1905.
[10] Hendradinata and Mahendra, "Analisis pengaruh resirkulasi udara pada kabin evaporator terhadap performansi mesin refrigerasi kompresi uap air conditioner dengan refrigeran R134a," Petra, vol. 2, no. 1, pp. 5–8, 2016.
[11] Jaipur National University, Energy Efficiency in Electrical Utilities. 2013.
[12] PT Rokindo Jaya Mandiri, "Perbedaan jenis compressor dan fungsinya pada sistem pendingin," [Online]. Available: https://www.rokindojayamandiri.com/blog-post/perbedaan-jenis-compressor-dan-fungsinya-pada-sistem-pendingin/. [Accessed: Jun. 22, 2023].
[13] M. R. Ramdhani, R. Muliawan, and N. Khakim, "Analisis pengaruh variasi kecepatan fan kondenser terhadap performansi sistem brine cooling untuk pembuatan es balok," pp. 147–153, 2023.
[14] M. C. Storage, "Mandiri Cold Storage - Air Blast Freezer," [Online]. Available: https://mandiricoldstorage.com/air-blast-freezer/. [Accessed: Jun. 22, 2023].
[15] D. Suwandi and R. Mulyani, "Pengaruh kecepatan fan kondensor terhadap kinerja pada mesin AC mobil," Prosiding Seminar Nasional, vol. 6, no. 1, pp. 502–510, 2020. Available: https://proceeding.isas.or.id /index.php/sentrinov/article/view/371.
[16] Syawalluddin and Muhaemin, "Analisa pengaruh arus aliran udara masuk evaporator terhadap coefficient of performance," Sintek Jurnal Teknik Mesin, vol. 7, no. 1, pp. 77–86, 2006.
[17] T. Muliawan et al., "Analisis performansi AC split dengan perbandingan refrigerant R410a dan R32 berdasarkan variasi putaran fan evaporator," Jurnal Jurusan Teknik Pendingin dan Tata Udara, Politeknik Negeri Indramayu, vol. 29, pp. 647–655, 2019. Available: http://jurnal.una.ac.id/ index.php/semnasmudi/article/download/941/836.
[18] A. Yani, Y. H. Anoi, and M. Prastiawan, "Analisis pengaruh penambahan fan pada instalasi air conditioner dan putaran engine terhadap temperatur cabin dan coefficient of performance," Turbo: Jurnal Program Studi Teknik Mesin, vol. 8, no. 1, pp. 40–47, 2019. DOI: 10.24127/trb.v8i1.918.